ARTICLE IN PRESS

Available online at www.sciencedirect.com

SCIENCE DIRECT®

ELSEVIER

Coastal Engineering xx (2005) xxx – xxx

Coastal Engineering
An International Journal for Coastal, Harbour and Offshore Engineers

www.elsevier.com/locate/coastaleng

The WRT method for the computation of non-linear four-wave interactions in discrete spectral wave models

Gerbrant Ph. van Vledder

Alkyon Hydraulic Consultancy and Research, P.O. Box 248, 8300 AE Emmeloord, The Netherlands

Abstract

An overview is given of the WRT method for the computation of weakly resonant non-linear four-wave interactions in a gravity wave spectrum and its application in discrete spectral wave models. The WRT method is based on Webb's [Webb, D.J., 1978. Nonlinear transfer between sea waves. Deep-Sea Res., 25, 279–298.] transformation of the Boltzmann integral and the numerical method introduced by Tracy and Resio [Tracy, B.A., Resio, D.T., 1982. Theory and calculation of the nonlinear energy transfer between sea waves in deep water. WIS technical report 11. US Army Engineer Waterways Experiment Station, Vicksburg, Mississippi, USA, 47 pp.]. It is shown that Webb's method produces an attractive set of integrable equations. Moreover, the Jacobian term arising from the integration over the frequency delta-function in the Boltzmann integral has a singularity well outside the energy containing part of the wave spectrum. A description is given of methods for computing the integration space for a given discrete spectral grid, both for deep and finite depth water. Thereafter, the application of Webb's method to discrete spectral wave models is described, followed by a summary of techniques reducing the computational workload while retaining sufficient accuracy. Finally, some methods are presented for the optimal inclusion of the WRT method in operational discrete spectral wave prediction models.

Keywords: WRT method; Wave spectrum; Quadruplets; Non-linear interactions; Wave model; Diagonal term

1. Introduction

The prediction of wind-generated waves is important for the design and safety of many offshore and nearshore structures and for the study of ocean surface related physical processes. Important tools for the prediction of these waves are third generation discrete spectral models. These models compute the evolution of wave action density $N=N(t,x,y,k,\theta)$ as a function of time t, space x and y, wave number k and direction θ. This evolution can be described with the action balance equation

$$\frac{\partial N}{\partial t}+\frac{\partial}{\partial x}\left(c_{g,x}N\right)+\frac{\partial}{\partial y}\left(c_{g,y}N\right)+\frac{\partial}{\partial k}\left(c_kN\right)+\frac{\partial}{\partial \theta}\left(c_\theta\right)=S_{\text{tot}}. \tag{1}$$

The c-terms represent the rate of change of action density in spatial or spectral space. The term S_{tot} on the right hand side of this equation is the source term, describing the changes in action density at each spectral component due to various physical processes. In present day third generation wave models, it is considered to be the sum of the following known individual physical processes

$$S_{\text{tot}}=S_{\text{inp}}+S_{\text{wcap}}+S_{\text{nl4}}+\left\{S_{\text{fric}}+S_{\text{brk}}+S_{\text{nl3}}+S_{\text{Bragg}}\right\}. \tag{2}$$

In this equation S_{inp} is the generation by wind, S_{wcap} is the dissipation by whitecapping, S_{nl4} are the non-linear four-wave interactions exchanging wave action between sets of four waves. The terms between the brackets become important in shallow water, where S_{fric} is bottom friction, S_{brk} is depth-limited wave breaking, S_{nl3} are non-linear interactions between sets of three waves and S_{Bragg} is the Bragg-scattering term.

The aim of such models is to represent each physical process in a source term as good as possible, preferably based on first principles. This is rather difficult for many physical processes; either because the underlying physics is poorly understood, which is the case for the dissipation by white-capping, or because the computational method is too time consuming, which is the case for the non-linear four-wave interactions. Consequently, many crude or incomplete parameterisations have been developed, each of which only applies for a limited range of conditions. In general, these parameterisations have a simple mathematical structure and are relatively

E-mail address: vledder@alkyon.nl.

0378-3839/$ - see front matter © 2005 Published by Elsevier B.V.
doi:10.1016/j.coastaleng.2005.10.011

easy to compute. Tuning of the models generally compensates for the deficiencies of these approximations.

The source term for non-linear four-wave interactions has a special place among the source terms, because so far it is the only source term that can be described by a closed set of equations derived on the basis of first principles.

It is nowadays widely accepted that weakly resonant non-linear four-wave interactions play an important role in the evolution of the energy spectrum of free surface gravity waves propagating at the ocean surface (cf. Phillips, 1981; Young and Van Vledder, 1993). Hasselmann (1962, 1963a,b) developed the theoretical framework for these interactions for a homogenous sea with a constant depth. He formulated an integral expression for the computation of these interactions, which is known as the Boltzmann integral for surface gravity waves. A few years later Zakharov (1968) derived an equivalent form, which is known as the kinetic equation. Both methods consider resonant interactions between sets of four wave numbers $\vec{k}_1$, $\vec{k}_2$, $\vec{k}_3$ and $\vec{k}_4$.

The computation of the Boltzmann integral is rather complicated and very time consuming since it requires the solution of a 3-fold integral over 3 wave number vectors. Because of this complexity it is (still) not feasible to include the full solution of the Boltzmann integral in operational spectral wave prediction models. Therefore, exact methods for computing the quadruplets are restricted to research models in which computational requirements are not a critical issue.

To overcome this disadvantage of exact methods, Hasselmann et al. (1985) developed the Discrete Interaction Approximation (DIA). They show that the DIA preserves a few but important characteristics of the full solution, such as the slow downshifting of the peak frequency and shape stabilisation during wave growth. The development of the DIA triggered the development of third generation wave prediction models, like the WAM model (WAMDIG, 1988), WaveWatch (Tolman, 1991), TOMAWAC (Benoit et al., 1996) and the SWAN model (Booij et al., 1999). The DIA was initially developed for deep water. The WAM group (WAMDIG, 1988) introduced a scaling technique to estimate the non-linear transfer for an arbitrary water depth. This technique contains a parameterisation of the magnitude scaling derived by Herterich and Hasselmann (1980).

In the last few years it became evident that the DIA shows some deficiencies (cf. Van Vledder et al., 2000). The DIA is not able to properly represent the non-linear transfer rate in comparison with exact solutions of the Boltzmann integral. For example, the DIA pumps too much energy from the spectral region near the spectral peak to higher frequencies. Van Vledder and Bottema (2002) showed that the present depth scaling does not include the inherent frequency dependent scaling behaviour. These known deficiencies of the DIA hamper the further development of source terms for third-generation discrete spectral models. Therefore, with continuing improvements in the description of the other processes and improved numerics, there is a strong need for replacing present approximate methods for the calculation of the quadruplet wave–wave interactions with methods that are both more accurate and computationally efficient.

The quality of the source term for the computation of the non-linear four-wave interactions in discrete spectral models can be improved in various ways. One approach is to improve the DIA by extending it with more and generally shaped interacting wave number configurations. This approach was already mentioned in Hasselmann et al. (1985), but not implemented due to operational limitations. The basic framework for extending the DIA is described in Van Vledder (2001). Examples of extending the DIA with more wave number configurations are given in Van Vledder et al. (2000), Hashimoto and Kawaguchi (2001), and Tolman (2004). The extension of the DIA with additional configurations is not straightforward since no optimal procedure has yet been found to select such configurations. A general drawback of extended DIA's is that a set of multiple configurations is only valid for a limited set of discrete spectra for which the coefficients of this set were determined, often by non-linear multi-variable optimisation methods.

Another approach is to speed up the computational methods for the exact computation of the non-linear transfer rate while retaining the basic properties of the computational method. This can be achieved by reducing the integration space in the evaluation of the Boltzmann integral, e.g. by filtering out small contributions or by using higher order quadrature methods. From a theoretical point of view the second approach is the most attractive since it does not involve tuning for a particular set of spectra. Therefore, one of these methods is the subject of this paper.

In literature various methods have been proposed to solve the Boltzmann integral by rewriting this integral to remove the δ-functions and to obtain a set of integrable equations. Hasselmann and Hasselmann (1981) were among the first to develop such a method. They rewrote the Boltzmann integral into a symmetric form and incorporated their method in the EXACT-NL model (Hasselmann and Hasselmann, 1985a). Their method explores symmetries and filtering techniques to efficiently compute the non-linear transfer rate for similarly shaped spectra. The first step in their method is choosing a representative reference spectrum for which the full non-linear transfer rate is computed. In the next step unimportant contributions to the transfer integral are filtered out. The filtered set of contributions can then be used to compute the non-linear transfer rate for similarly shaped spectra. A drawback of this method is that when a spectrum deviates too much from the reference spectrum, a new reference spectrum must be defined and the Boltzmann integral must be re-computed and the contributions must be re-filtered. Weber (1988), Van Vledder (1990) and Van Vledder and Holthuijsen (1993) used the EXACT-NL model in various studies of the evolution of the wave spectrum. A description of applying this computational technique can be found in Van Vledder and Weber (1988).

Webb (1978) presented a set of equations to solve the Boltzmann equation. Using some analytical transformations he was able to eliminate the δ-functions in (6). Tracy and Resio (1982) incorporated the method of Webb (1978) in a computational method for discrete deep-water spectra. They

noted that different parts of the integration space are related via scaling laws, thus saving time in the preparatory phase of a computation of the non-linear transfer rate for a given spectrum. Resio and Perrie (1991), and Young and Van Vledder (1993) presented further applications of this method. Resio (1998) also developed a shallow water version of Webb's method, which was applied by Resio et al. (2001). This computational method is generally known as the WRT-method for the computation of the non-linear transfer rate due to non-linear four-wave interactions in a discrete wave spectrum. Lin and Perrie (1998) presented a Reduced Interaction Approximation (RIA), which is based on the WRT-method. In their method they restrict the integration space around a central wave number, thereby limiting the number of interacting wave number configurations.

Masuda (1980) proposed another set of equations for solving the Boltzmann integral for deep water. Like, Webb (1978), he applied a number of analytical transformations to eliminate the δ-functions in the Boltzmann integral, the basic difference between their methods being the pair of wave numbers considered at the highest level, with Webb (1978) using the pair $\left\{\vec{k}_1, \vec{k}_3\right\}$ and Masuda (1980) using the pair $\left\{\vec{k}_1, \vec{k}_2\right\}$. Hashimoto et al. (1998) extended Masuda's method to finite-depth water. Hashimoto et al. (2002) presented an application of this method in the SWAN model. Polnikov (1997) presented a modified Masuda method, whereas Lavrenov (2001) proposed a method that uses a combination of analytical transformations and numerical integration techniques to handle singularities arising from manipulations of the Boltzmann integral. Additional information about various computational methods can be found in Benoit (2005).

From the available methods, the one of Webb (1978) was selected for further improvements. Not only for its attractive set of equations, but also because the author is most familiar with this method and its numerical implementation developed by Tracy and Resio (1982).

The original WRT method was completely rewritten by the author as a set of subroutines for easy implementation in any third-generation wave prediction model and to use it as a starting point for optimisation in operational discrete spectral wave models. During this process, valuable theoretical and practical insights into its workings were obtained, which were included in a modified computational method for computing the non-linear four-wave interactions in operational discrete spectral wave models. This version of the WRT method has been implemented in various third generation wave prediction models, such as WaveWatch III (Tolman, 2002), SWAN (Booij et al., 2004), CREST (Ardhuin et al., 2001) and PROWAM (Monbaliu et al., 1999).

The aim of this paper is to give a comprehensive description of the method of Webb (1978), and its implementation in a discrete spectral wave model, to serve as a basis for further studies to increase the applicability of the WRT method. The remainder of this paper is divided into five parts. The first part contains an overview of the theory of non-linear four-wave interactions. The second part contains a detailed description of Webb's method for solving the Boltzmann integral. The third part describes how this method is applied to compute the non-linear transfer rate in a discrete wave spectrum. The fourth part addresses methods and associated parameter settings to improve the computational efficiency while retaining sufficient accuracy. Finally, the last part addresses the handling of the WRT method in operational wave model applications, and the treatment in areas with a varying bottom topography.

2. Theoretical background

Hasselmann (1962, 1963a,b) found that a set of four waves, called a quadruplet, could exchange energy when the following resonance conditions are satisfied

$$\vec{k}_1 + \vec{k}_2 = \vec{k}_3 + \vec{k}_4 \tag{3}$$

and

$$\omega_1 + \omega_2 = \omega_3 + \omega_4, \tag{4}$$

in which ω_i the radian frequency and $\vec{k}_i$ the wave number vector ($i=1,...,4$). The linear dispersion relation relates the radian frequency ω and the wave number k

$$\omega^2 = gk\tanh(kh). \tag{5}$$

Here, g is the gravitational acceleration and h the water depth. Hasselmann (1962, 1963a,b) describes the non-linear interactions between wave quadruplets in terms of their action density n, where $n=E/\omega$ and E the energy density. The rate of change of action density at a wave number $\vec{k}_1$ due to all quadruplet configurations involving $\vec{k}_1$ is

$$\begin{aligned}\frac{\partial n_1}{\partial t} = & \iiint G\left(\vec{k}_1, \vec{k}_2, \vec{k}_3, \vec{k}_4\right) \\ & \times \delta\left(\vec{k}_1 + \vec{k}_2 - \vec{k}_3 - \vec{k}_4\right) \\ & \times \delta(\omega_1 + \omega_2 - \omega_3 - \omega_4) \\ & \times [n_1 n_3(n_4 - n_2) + n_1 n_4(n_3 - n_1)]\mathrm{d}\vec{k}_2\mathrm{d}\vec{k}_3\mathrm{d}\vec{k}_4\end{aligned} \tag{6}$$

where $n_i = n\left(\vec{k}_i\right)$ is the action density at wave number $\vec{k}_i$ and G is the coupling coefficient. The δ-functions in (6) ensure that contributions to the integral only occur for quadruplets satisfying the resonance conditions. The δ-functions also ensure conservation of wave energy, wave action and wave momentum.

The coupling coefficient G is given by

$$G\left(\vec{k}_1, \vec{k}_2, \vec{k}_3, \vec{k}_4\right) = \frac{9\pi g^2 D^2\left(\vec{k}_1, \vec{k}_2, \vec{k}_3, \vec{k}_4\right)}{4\rho^2\omega_1\omega_2\omega_3\omega_4}. \tag{7}$$

In this expression $D\left(\vec{k}_1, \vec{k}_2, \vec{k}_3, \vec{k}_4\right)$ is the interaction coefficient, and ρ is the density of water. The deep-water expression for the interaction coefficient was first given by Hasselmann (1962). Webb (1978) used an algebraic manipulator to simplify the mathematical structure of this coefficient. However, his expression contained some misprints. Corrected

expressions are given in Dungey and Hui (1979). Herterich and Hasselmann (1980) derived a finite depth version of the interaction coefficient. Zakharov (1999) re-derived the coupling coefficients for deep and finite depth water, and expressed them in a form similar to those of Webb (1978). Gorman (2003) provides a detailed analysis of the finite depth interaction coefficient and he derived expressions for the treatment of discontinuities therein.

The difference between exact methods and the DIA is best illustrated by means of the interaction diagram proposed by Hasselmann (1968b) to visualize the integration space. In exact methods the integration space consists of all possible combinations of resonant sets of four wave numbers. Following Hasselmann (1968b) these sets can be grouped in pairs with the same sum for their frequencies. For deep water, where the dispersion relation reduces to $\omega^2 = gk$, the resonance conditions (3) and (4) become

$$\vec{k}_1 + \vec{k}_2 = \vec{k}_3 + \vec{k}_4 = \vec{k} \tag{8}$$

$$\sqrt{k_1} + \sqrt{k_2} = \sqrt{k_3} + \sqrt{k_4} = \gamma\sqrt{k}. \tag{9}$$

For a fixed value of γ all sets of wave numbers satisfying the resonance conditions lie on a specific curve. A collection of these curves is illustrated in Fig. 1. In this figure it can be seen that moving the points P and Q independently of one another along a curve generates many resonant wave number configurations. This procedure can be repeated for all other curves generating even more resonant wave number configurations.

For the DIA, however, only one wave number configuration (and its mirror image) are considered. They lie on the curve with $\gamma = \sqrt{2}$. The shape of each configuration is determined by the shape parameter λ. In this configuration $\vec{k}_1 = \vec{k}_2 = \vec{k}$, $k_3 = (1+\lambda)^2 k$ and $k_4 = (1-\lambda)^2 k$, with $\lambda = 0.25$ as used in the WAM model (WAMDIG, 1988). These configurations are illustrated in Fig. 2. This implies that the DIA uses only a subset (one point on a curve) of a subset (one curve) of all possible wave number configurations compared to exact methods. The typical difference in number

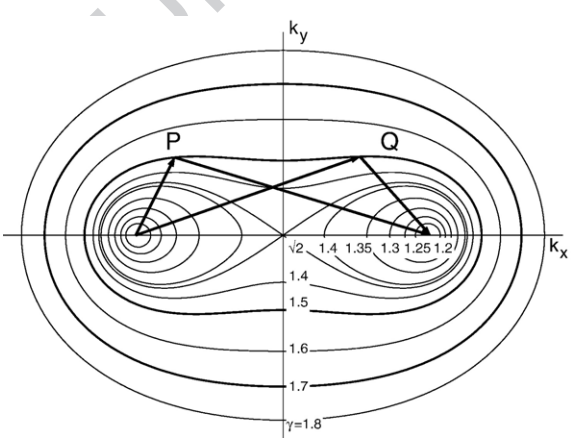

Fig. 1. Interaction diagram for a given value of $\vec{k}_1 + \vec{k}_2 = \vec{k}_3 + \vec{k}_4 = \vec{k}$. Each curve is for a specific value of γ (after Phillips, 1960; Hasselmann, 1963b).

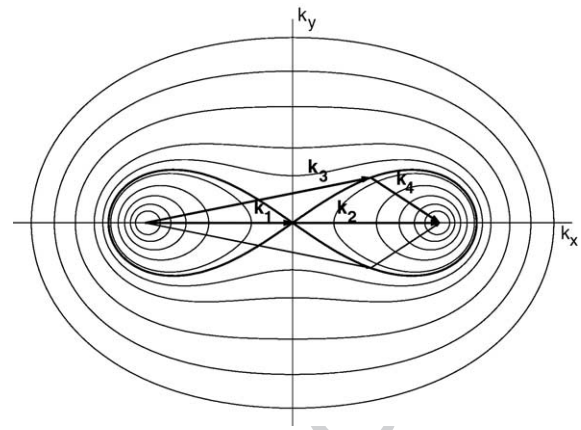

Fig. 2. Position of wave number configuration for the Discrete Interaction Approximation with $\lambda = 0.25$ and its mirror image in the interaction diagram.

of configurations in model applications is about three to four orders of magnitude.

3. Webb's method

3.1. Basic equations

The method of Webb is based on a number of analytical transformations to remove the δ-functions in the Boltzmann integral. The main choice in Webb's method is to consider the integration space for each $\left(\vec{k}_1, \vec{k}_3\right)$ combination. This implies that (6) can be written as

$$\frac{\partial n_1}{\partial t} = \int \mathrm{d}\,\vec{k}_3 T\left(\vec{k}_1, \vec{k}_3\right) \tag{10}$$

in which the function T is given by

$$T\left(\vec{k}_1, \vec{k}_3\right) = \iint \mathrm{d}\,\vec{k}_2 \mathrm{d}\,\vec{k}_4 \times G \times \delta\left(\vec{k}_1 + \vec{k}_2 - \vec{k}_3 - \vec{k}_4\right) \times \delta(\omega_1 + \omega_2 - \omega_3 - \omega_4) \times [n_1 n_3 (n_4 - n_2) + n_2 n_4 (n_3 - n_1)]. \tag{11}$$

In the following the product of action densities is written as

$$N_{1,2,3,4} = [n_1 n_3 (n_4 - n_2) + n_2 n_4 (n_3 - n_1)]. \tag{12}$$

The δ-function over the wave numbers is eliminated by writing $\vec{k}_4$ as

$$\vec{k}_4 = \vec{k}_1 + \vec{k}_2 - \vec{k}_3. \tag{13}$$

The integral $T\left(\vec{k}_1, \vec{k}_3\right)$ then becomes

$$T\left(\vec{k}_1, \vec{k}_3\right) = \int \mathrm{d}\,\vec{k}_2 \times \delta\left(\Delta\omega_{1,2,3,\vec{k}_1+\vec{k}_2-\vec{k}_3}\right) \times G \times N_{1,2,3,4} \tag{14}$$

in which the frequency mismatch is written as

$$\Delta\omega_{1,2,3,\vec{k}_1+\vec{k}_2-\vec{k}_3} = \omega_1 + \omega_2 - \omega_3 - \omega_{\vec{k}_1+\vec{k}_2-\vec{k}_3}. \tag{15}$$

To eliminate the remaining δ-function, it is noted that the locations in wave number space where $\Delta\omega_{1,2,3,\vec{k}_1+\vec{k}_2-\vec{k}_3} = 0$ trace out a closed curve, which is referred to as a locus.

Following Tracy and Resio (1982) and Rasmussen (1998), the integration vector $\vec{k}_2$ is resolved in two components such that one is tangential to the locus $\vec{k}_{2,t}$ and one, which is normal to that locus $\vec{k}_{2,n}$. The Jacobian of this transformation is 1. Tracy and Resio (1982) denoted this local co-ordinate system with the components $(\vec{s}, \vec{n})$. This transformation is convenient since it allows making use of the following property of the δ-function

$$\int \delta(f(x))\mathrm{d}x = \left|\frac{\partial f}{\partial x}\right|^{-1}_{f(x)=0} \tag{16}$$

Integration over the δ-function then yields

$$T\left(\vec{k}_1, \vec{k}_3\right) = \iint \mathrm{d}\,\vec{k}_{2,t}\mathrm{d}\,\vec{k}_{2,n} \times J \times G \times N_{1,2,3,4} \tag{17}$$

with J the Jacobian of this transformation. It is defined as

$$J = \left|\frac{\partial \Delta\omega_{1,2,3,\vec{k}_1+\vec{k}_2-\vec{k}_3}}{\partial\,\vec{k}_{2,n}}\right|^{-1}. \tag{18}$$

Since $\partial\Delta\omega_{1,2,3,\vec{k}_1+\vec{k}_2-\vec{k}_3}/\partial\,\vec{k}_{2,t} = 0$, the Jacobian J can be obtained from the gradient of the frequency mismatch. Since $\vec{k}_1$ and $\vec{k}_3$ are fixed, the gradient $\nabla_{\vec{k}_2}\Delta\omega_{1,2,3,\vec{k}_1+\vec{k}_2-\vec{k}_3}$ can be written as

$$\Delta_{\vec{k}_2}\omega_{1,2,3,\vec{k}_1+\vec{k}_2-\vec{k}_3} = \nabla_{\vec{k}_2}\omega_2 - \nabla_{\vec{k}_2}\omega_{\vec{k}_1+\vec{k}_2-\vec{k}_3}. \tag{19}$$

Applying the chain rule for differentiation yields

$$\begin{aligned}\nabla_{\vec{k}_2}\Delta\omega_{1,2,3,\vec{k}_1+\vec{k}_2-\vec{k}_3} &= \nabla_{\vec{k}_2}\omega_2 \\ &\quad - \nabla_{\vec{k}_2}\left(\vec{k}_1+\vec{k}_2-\vec{k}_3\right)\nabla_{\vec{k}_1+\vec{k}_2-\vec{k}_3}\omega_{\vec{k}_1+\vec{k}_2-\vec{k}_3} \\ &= \vec{c}_{g,2} - \vec{c}_{g_{\vec{k}_1+\vec{k}_2-\vec{k}_3}}.\end{aligned} \tag{20}$$

with $\vec{c}_{g,i}$ the group velocity for the wave number vector $\vec{k}_i$. Therefore, the Jacobian J can be written as:

$$J = \left|\vec{c}_{g,2} - \vec{c}_{g_{\vec{k}_1+\vec{k}_2-\vec{k}_3}}\right|^{-1}. \tag{21}$$

Rasmussen (1998) was the first to obtain this elegant result. In Tracy and Resio (1982) the Jacobian term J is referred to as the gradient term or phase term.

From a historical point of view it is interesting to note that Tracy and Resio (1982) derived the Jacobian term using the Cartesian components of the wave number $\vec{k}_2$, but also that expression (21) is hidden in their result. This equivalence is illustrated in Appendix A.

As expressed by (21) the Jacobian J has some nice properties; it has the same analytical form for deep and shallow water, and it is symmetric in its components. The term J becomes unbounded only when $\vec{k}_2 = \vec{k}_4$, including the singular case $\vec{k}_1 = \vec{k}_2 = \vec{k}_3 = \vec{k}_4$. It is non-zero for all other solutions of the resonance conditions.

Webb (1978) noted that for symmetry reasons the integration space in Eq. (11) can be reduced by a factor 2. Since the Boltzmann integral is symmetric with respect to inter-changing the variables $\vec{k}_1$ and $\vec{k}_2$, or $\vec{k}_3$ and $\vec{k}_4$, part of the integration space can be omitted where the wave number $\vec{k}_1$ is closer to wave number $\vec{k}_4$ than to wave number $\vec{k}_3$. Mathematically, this is achieved with the Heaviside function $H(x)$:

$$H(x) = \begin{cases} 1 & \text{if} \quad x > 0 \\ 0 & \text{if} \quad x < 0 \end{cases} \tag{22}$$

and

$$x = |\,\vec{k}_1 - \vec{k}_4| - |\,\vec{k}_1 - \vec{k}_3|. \tag{23}$$

The reduction in integration space is compensated by a factor 2 in the integral expression. Thus

$$\begin{aligned}T\left(\vec{k}_1, \vec{k}_3\right) = 2\int \mathrm{d}\,\vec{k}_{2,t}G \times \left|\vec{c}_{g,2} - \vec{c}_{g_{\vec{k}_1+\vec{k}_2-\vec{k}_3}}\right|^{-1} \\ \times\ H\left(\vec{k}_1 - \vec{k}_4| - |\,\vec{k}_1 - \vec{k}_3\right) \times N_{1,2,3,4}.\end{aligned} \tag{24}$$

Following Tracy and Resio (1982), expression (24) can be written as a closed line integral with the variable s along the locus instead of the tangential component $\vec{k}_{2,t}$.

In the following the Heaviside function is omitted in the formulation of the term T, unless stated otherwise

$$T\left(\vec{k}_1, \vec{k}_3\right) = \int_s \mathrm{d}s \times G \times J \times N_{1,2,3,4}. \tag{25}$$

The subscript s indicates that the integration is to be performed around the locus as a function of the coordinate s.

3.2. The integration space

In the WRT method the integration space needs to be determined for each combination of the wave number vectors $\vec{k}_2$ and $\vec{k}_3$. In this section a geometric method is outlined to find this integration space. For a given $\left(\vec{k}_1, \vec{k}_3\right)$ wave number combination all possible $\vec{k}_2$ and $\vec{k}_4$ combinations can easily be found on the basis of geometric considerations. The purpose of this geometric method is to find all wave number vectors $\vec{k}_2$ and $\vec{k}_4$ such that

$$\vec{k}_1 + \vec{k}_2 = \vec{k}_3 + \vec{k}_4. \tag{26}$$

The first step of this method is to choose a wave number magnitude $\vec{k}_2$. (Below it will be shown that only $\vec{k}_2$ values in a certain range produce valid solutions.) Since the direction θ_2 of $\vec{k}_2$ is not yet known, the end point of the sum vector $\vec{k}_1 + \vec{k}_2$ forms a circle with radius k_2 and centre at $\vec{k}_1$. Similarly, a circle can be drawn for the wave number $\vec{k}_4$, with radius k_4 and centre at $\vec{k}_3$. The crossing points of the two circles are by definition solutions of the resonance conditions. An example of this geometric procedure is shown in Fig. 3. The radius k_4 can easily be computed from the resonance condition (4). For given radian frequencies ω_1,ω_2 and ω_3 the wave number k_4 is computed from

$$(\omega_1 + \omega_2 - \omega_3)^2 = gk_4\,\tanh(k_4 h). \tag{27}$$

An efficient and explicit solution technique for this equation is given in Hunt (1979), who derived an accurate 9-point Padé approximation, which is applicable in deep and shallow water.

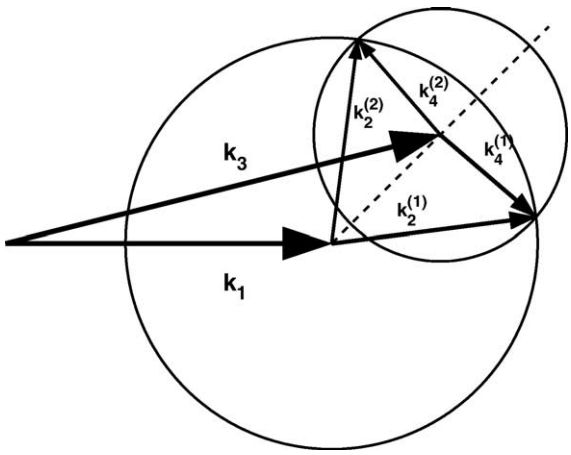

Fig. 3. Illustration of the geometric solution technique for the resonance conditions for given wave numbers $\vec{k}_1$ and $\vec{k}_3$.

The resulting system of equations equivalent to (26) is

$$\begin{aligned} k_{1,x} + k_2\cos(\theta_2) &= k_{3,x} + k_4\cos(\theta_4) \\ k_{1,y} + k_2\sin(\theta_2) &= k_{3,y} + k_4\sin(\theta_4) \end{aligned} . \tag{28}$$

Following Tracy and Resio (1982) the difference vector $\vec{P} = \vec{k}_1 - \vec{k}_3$ is introduced, see Fig. 4. Using the components of this vector and rearranging the equations gives

$$\begin{aligned} P_x + k_2\cos(\theta_2) &= k_4\cos(\theta_4) \\ P_y + k_2\sin(\theta_2) &= k_4\sin(\theta_4) \end{aligned} . \tag{29}$$

Next the direction θ_p and magnitude P of this vector are introduced with $\vec{P} = P(\cos(\theta_p), \sin(\theta_p))$ and $P = |\vec{P}|$, respectively. Squaring and summing the equations in (29) gives after some straightforward algebraic manipulations

$$\frac{k_4^2 - k_2^2 - P^2}{2k_2P} = \cos(\theta_2 - \theta_p). \tag{30}$$

Solving (30) for θ_2 gives two solutions of the resonance conditions

$$\theta_2 = \theta_p \pm \mathrm{acos}\left(\frac{k_4^2 - k_2^2 - P^2}{2k_2P}\right). \tag{31}$$

Once the wave numbers $\vec{k}_2$ are known, the corresponding solutions for the wave numbers $\vec{k}_4$ are easily computed from

$$\vec{k}_4 = \vec{P} + \vec{k}_2. \tag{32}$$

The valid solutions of Eq. (31) trace out a closed curve in wave number space, which is referred to as the locus. For a given wave number pair $(\vec{k}_1, \vec{k}_3)$ with $\vec{k}_1 \vec{k}_3$ the loci for the wave numbers $\vec{k}_2$ and $\vec{k}_4$ are closed egg-shaped curves (Webb, 1978; Tracy and Resio, 1982; Young and Van Vledder, 1993). An example of such loci for the wave numbers $\vec{k}_2$ and $\vec{k}_4$ is given in Fig. 4. It can be seen that the wave numbers $\vec{k}_3$ and $\vec{k}_1$ lie on the loci for the wave numbers $\vec{k}_2$ and $\vec{k}_4$, respectively since they are solutions of the resonance conditions. The locus is symmetric around a line through the origin with direction θ_p.

Eq. (31) was also derived in Van Vledder (2000), where it is referred to as the polar method for obtaining solutions of the resonance conditions. The geometric approach was referred to in Khatri and Young (1999), but no equations or clear diagrams were presented therein.

A special solution of the resonance conditions is obtained for the case where $\vec{k}_1 = \vec{k}_3$ but with $\theta_1 \neq \theta_3$. Subsequently $k_2 = k_4$ and Eq. (31) reduces to

$$\theta_2 = \theta_p \pm \mathrm{acos}\left(\frac{-P}{2k_2}\right). \tag{33}$$

Varying the wave number k_2 and choosing the 'plus' or the 'minus' sign produces a straight line representing a solution of the resonance conditions. Since the wave numbers $\vec{k}_2$ and $\vec{k}_4$ are interchangeable, the solution for wave number $\vec{k}_4$ can be found by choosing the 'minus' or 'plus' sign in (33). This solution is also a straight line, parallel to the solution for $\vec{k}_2$. The direction θ_s of these lines is equal to

$$\theta_s = \frac{1}{2}(\theta_1 + \theta_3). \tag{34}$$

An example solution is illustrated in Fig. 5. An alternative expression for θ_2 is obtained by substitution of $\vec{k}_4 = \vec{k}_2$ in (29). Rearranging the terms gives

$$\begin{aligned} P_x &= k_2(\cos(\theta_4) - \cos(\theta_4)) \\ P_y &= k_2(\sin(\theta_4) - (\sin(\theta_4)). \end{aligned} \tag{35}$$

This leads to

$$P^2 = 2k_2^2(1 - \cos(\theta_2 - \theta_4)). \tag{36}$$

Since $\theta_s = \frac{1}{2}(\theta_2 + \theta_4)$, the angle θ_2 is given by

$$\theta_2 = \theta_s \pm \frac{1}{2}\mathrm{acos}\left(1 - \frac{P^2}{2k_2^2}\right). \tag{37}$$

A similar procedure as above can be followed to obtain solutions of the resonance conditions, which also consist of two straight parallel lines.

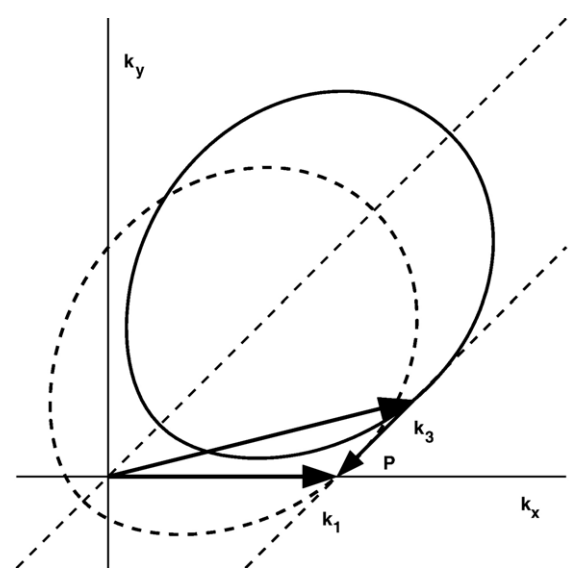

Fig. 4. Example of a locus for a given wave number configuration $\vec{k}_1$ and $\vec{k}_3$.

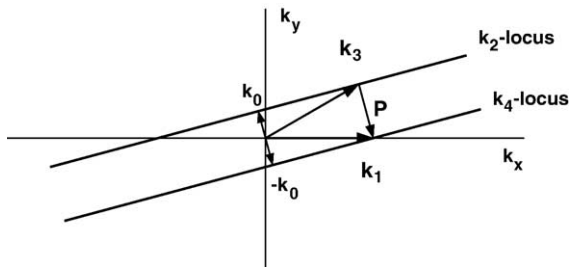

Fig. 5. Example of a locus for the special case where the vectors $\vec{k}_1$ and $\vec{k}_3$ have equal lengths but different directions.

The main difference between the expressions (37) and (33) is the fact that the directions θ_p and θ_s are perpendicular to one another. In practise, no preference is given to either one of these methods for generating these special solutions of the resonance conditions.

3.3. Methods for computing the loci

Various methods have been proposed for the determination of the locus for a given pair of wave numbers $\vec{k}_1$ and $\vec{k}_3$. All of these methods are based on solving the locus equation

$$W\left(\vec{k}_2\right) = \omega_1 + \omega_2 - \omega_3 - \omega_{\vec{k}_1+\vec{k}_2-\vec{k}_3} = 0. \tag{38}$$

Tracy and Resio (1982) presented a radial method for determining points on the locus. They first determine a central wave number $\vec{k}_c$ inside the locus on the axis of symmetry. Then, starting from this point, a set of lines is projected outwards with increasing angles using a constant angular step $\Delta\theta$. The locations on these radial lines, where the locus function is zero, are by definition points on the locus. The position of the zero-crossings is determined by an iterative root-finding procedure since no explicit expression exists to obtain the locations of these zero-crossings. The number of points N_{loc} on the locus and the angular step $\Delta\theta$ are related as $N_{\mathrm{loc}}=2\pi/\Delta\theta$. An example of their method is shown in panel (a) of Fig. 6.

Tracy and Resio (1982) choose the central point as $\vec{k}_c = -\vec{P}$, which is the point on the axis of symmetry where the locus function has its maximum, both for deep and shallow water. Van Vledder (2000) showed that in shallow water this choice for the central point shifts to one side of the locus. This has the disadvantage that, when used with constant $\Delta\theta$, the radial method produces a highly uneven distribution of points on the locus. To avoid this unevenness, he suggests choosing the central point $\vec{k}_c$ halfway along the crossing points of the locus with the axis of symmetry.

Van Vledder (2000) presented a polar method to determine discrete points on the locus. His method uses circles around the origin with an increasing radius k_2. The locations on these circles where the locus function is zero are by definition points on the locus. In contrast to the radial method of Tracy and Resio (1982), the zero-crossings can be determined by an explicit expression, viz. Eq. (31) presented above. Only values in a certain range of k_2 lead to a valid solution of (31). For deep water Tracy and Resio (1982) and Van Vledder (2000) give

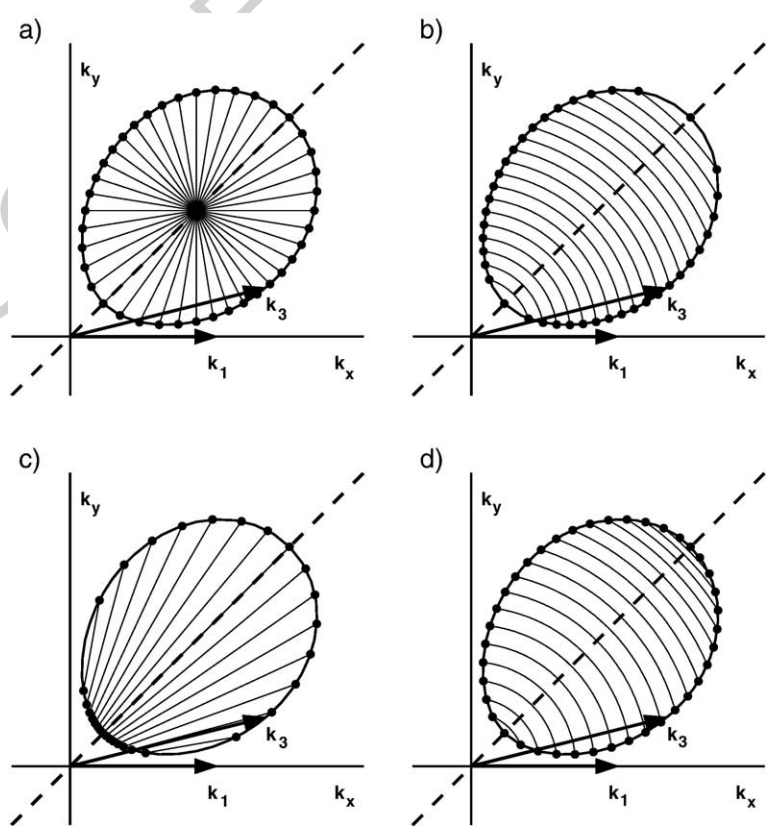

Fig. 6. Example of methods for computing the locus for a given wave number combination of $\vec{k}_1$ and $\vec{k}_3$. Panel (a) radial method of Tracy and Resio (1982), panel (b) polar method of Van Vledder (2000), panel (c) modified polar method of Prabhakar and Pandurangan (2004), panel (d) polar method with equidistant spacing.

explicit expressions for the minimum (k_A) and maximum (k_B) values of k_2, which lie on the axis of symmetry. They are

$$k_A = \left(\frac{-q + \sqrt{2P - q^2}}{2} \right)^2 \tag{39}$$

and

$$k_B = \left(\frac{-P - q^2}{2q} \right)^2 . \tag{40}$$

In these equations $q = k_1^{1/2} - k_3^{1/2}$. For finite depth the values for k_A and k_B need to be found by iteration. See Fig. 7 for a definition sketch of these variables. Varying the wave number k_2 between these limits produces all valid solutions of the resonance conditions.

Various methods exist of choosing intermediate k_2-values between the limits k_A and k_B for computing points on the locus. The simplest one is a linear distribution of k_2-values

$$k_{2,i} = k_A + (i-1)\Delta k_2 \quad \text{for} \quad i = 1, N_{k_2} \tag{41}$$

in which the step size Δk_2 is related to the number of points N_{k_2} on the symmetry axis of the locus according to

$$\Delta k_2 = \frac{k_B - k_A}{N_{k_2} - 1} . \tag{42}$$

The number of points on the locus is related to the number of k_2 values on the symmetry axis according to $N_{loc} = 2(N_{k_2} - 1)$. An example of the polar method is shown in panel (b) of Fig. 6. One may also think of using a geometric spacing of k_2-values, to better reflect the geometric spacing of commonly used geometrically spaced spectral grids. In this method

$$k_{2,i} = \lambda^{i-1} k_A \quad \text{for} \quad i = 1, N_{k_2} \tag{43}$$

such that

$$k_b = \lambda^{N_{k_2}-1} k_A . \tag{44}$$

Here, the value of λ is linked to the ratio of subsequent wave numbers in the spectral grid of the discrete wave spectrum such that $\lambda \approx k_{i+1}/k_i$. The above-mentioned argument for choosing a geometric spacing does not hold for the points on the k_4-locus. Since the distribution of points on the k_4-locus is linked with those on the k_2-locus, they do not follow the local variation of wave numbers of the spectral grid (cf. Fig. 8).

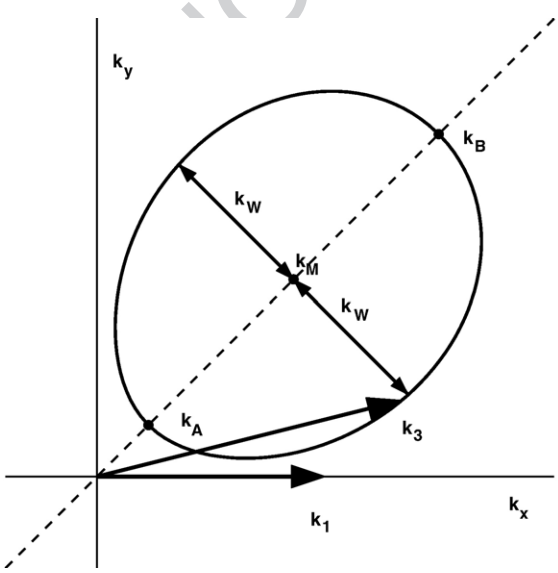

Fig. 7. Definition sketch for properties of a locus.

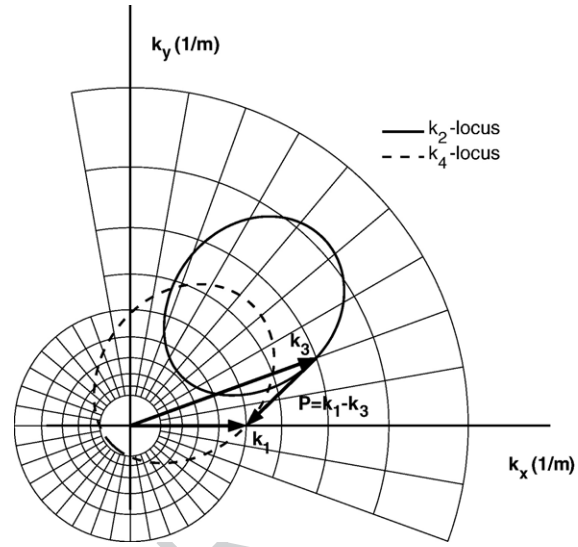

Fig. 8. Illustration of the position of the $\vec{k}_2$ and $\vec{k}_4$ loci in a discrete spectral polar grid with geometric spacing of wave numbers and a constant angular spacing.

Recently, Prabhakar and Pandurangan (2004) presented another explicit method for obtaining the points on the locus. For deep water and for given wave numbers $\vec{k}_1$ and $\vec{k}_3$ and a given angle θ_2, they rewrote the locus Eq. (38) as a cubic equation in the wave number k_2. By varying the angle θ_2 with a constant step $\Delta\theta_2$, they obtained pairs of discrete points on the locus. An example of results of their method is shown in panel (c) of Fig. 6. From this figure it directly follows that the range of θ_2 is limited to a small sector and that for each θ_2 two values for k_2 are found. A disadvantage of their method is that it has a coarser resolution on the locus where θ_2 is almost equal to the local direction on the locus.

All of the above methods produce a variable spacing of points on the locus. To obtain a constant spacing of points on the locus, Van Vledder (2000) proposed an adaptive technique based on his explicit polar method. An example of this method is shown in panel (d) of Fig. 6. The spacing and the number of points on the locus can be obtained from an estimate of the circumference of the locus. A good approximation of this circumference is obtained by assuming the locus to be an ellipse with principal semi-axes equal to $\frac{1}{2}(k_A - k_B)$ and k_W, with k_W the width of the locus at the point $k_M = \frac{1}{2}(k_A + k_B)$ halfway the symmetry axis. See Fig. 7 for a definition sketch.

Each of these methods is able to produce a sufficiently fine distribution of points on the locus when the number of points exceeds, say, 50. From these methods, the explicit polar method of Van Vledder (2000) is favoured because of its simplicity. Further, an equidistant spacing of points is recommended to obtain a regular distribution of points on the loci for both the wave numbers $\vec{k}_2$ and $\vec{k}_4$.

3.4. Computation of the special solution

For the special case $k_1 = k_3$ and $\theta_1 \neq \theta_3$, the solution of the resonance conditions consists of two parallel lines for the wave numbers $\vec{k}_2$ and $\vec{k}_4$. These lines have a direction θ_s as specified by Eq. (34). These lines can therefore be parameterised as

$$\vec{k}_2 = \vec{k}_0 + \mu \begin{pmatrix} \cos(\theta_s) \\ \sin(\theta_s) \end{pmatrix} \tag{45}$$

and

$$\vec{k}_4 = -\vec{k}_0 + \mu \begin{pmatrix} \cos(\theta_s) \\ \sin(\theta_s) \end{pmatrix}. \tag{46}$$

In the Eqs. (45) and (46) $\vec{k}_0$ is a point on the $\vec{k}_2$-line. The magnitude of this vector is equal to the shortest distance of the lines to the origin. As shown in Fig. 5, geometric considerations indicate that the magnitude of $\vec{k}_0$ is equal to

$$k_0 = \frac{P}{2} \tag{47}$$

or, equivalently

$$k_0 = k_1 \sin\left(\frac{1}{2}(\theta_3 - \theta_1)\right). \tag{48}$$

The first value also follows by equating the term in the brackets in Eq. (33), or the one in Eq. (37), to -1. The direction of the vector $\vec{k}_0$ is perpendicular to θ_s. Thus

$$\vec{k}_0 = \frac{P}{2} \begin{pmatrix} -\sin(\theta_s) \\ \cos(\theta_s) \end{pmatrix}. \tag{49}$$

The length of these lines should be large enough to cover the energy containing part of the spectrum. Therefore, it is recommended to choose the range of the parameter μ at least from $-k_{\max}$ to $+k_{\max}$, where $k_{\max}$ is the maximum discrete wave number. Considerations for choosing $k_{\max}$ are given in the Next section.

4. Computational technique

4.1. Discretisation

To compute the non-linear transfer rate for a given discrete wave spectrum, it is assumed that this wave spectrum is given in terms of a discrete action density spectrum as a function of the discrete wave numbers k_i (for $i = 1, N_k$) and directions $\theta_j (j = 1, N_\theta)$ with a constant spacing $\Delta\theta$. Based on expression (10) the change of action density at a certain discrete wave number ($k_{i_{kl}}$, $\theta_{j_{kl}}$) is expressed as

$$\Delta n\left(k_{i_{kl}}, \theta_{j_{kl}}\right) = \sum_{i_{k3}=1}^{N_k} \sum_{j_{\theta 3}=1}^{N_\theta} k_{i_{k3}} T\left(k_{i_{kl}}, \theta_{i_{kl}}, k_{i_{k3}}, \theta_{j_{k3}}\right) \Delta k_{i_{k3}} \Delta\theta$$
$$\text{for} \quad i_{kl} = 1, N_k \quad \text{and} \quad j_{\theta 1} = 1, N_\theta. \tag{50}$$

in which the factor $k_{i_{k3}}$ is the Jacobian term arising from the transformation from $\vec{k}_3$ to (k_3, θ). The singular point where $\vec{k}_1 = \vec{k}_3$ (and $\vec{k}_2 = \vec{k}_4$) is omitted in the evaluation of expression (50). Herterich and Hasselmann (1980) and Gorman (2003) suggest that ignoring this contribution leads to a negligible contribution to the total transfer rate.

A useful property of the T-function is

$$T\left(\vec{k}_1, \vec{k}_3\right) = -T\left(\vec{k}_3, \vec{k}_1\right). \tag{51}$$

This property allows computing only half of all possible combinations in (50), since symmetric storing of the contributions to the non-linear transfer rate can be used according to

$$\begin{aligned} \Delta n(i_{kl}, j_{kl}) &= T\left(\vec{k}_1, \vec{k}_3\right) k_{i_{k3}} \Delta k_{i_{k3}} \Delta\theta \\ \Delta n(i_{k3}, j_{k3}) &= -T\left(\vec{k}_1, \vec{k}_3\right) k_{il} \Delta k_{i_{kl}} \Delta\theta. \end{aligned} \tag{52}$$

The term $T\left(\vec{k}_1, \vec{k}_3\right)$ can be discretized as

$$\begin{aligned} T\left(\vec{k}_1, \vec{k}_3\right) &= \oint_s G(s) J(s) N(s) \mathrm{d}s \\ &\approx \sum_{i=1}^{N_s} G(s_i) J(s_i) N(s_i) \Delta s_i. \end{aligned} \tag{53}$$

In (53) the terms G, J and N are written as functions of the local coordinate s along the locus.

The actual computation of the non-linear transfer rate for a given discrete spectrum consists of the integration of the product of three functions for each locus. The functions for the Jacobian term and the coupling coefficient are independent of the actual spectral values. Therefore, they can be pre-computed. The third function is the product term of the (interpolated) action densities. These action densities cannot be pre-computed and need to be computed for each spectrum for which the non-linear transfer rate is computed.

4.2. Interpolation

In evaluating expression (53) one should consider that the locus is given at discrete points. In general these points do not coincide with the discrete spectral grid points. The position of a k_2- and a k_4-locus in wave number space and its position in a discretized polar spectral grid are visualised in Fig. 8. The action densities at the points on the locus can be obtained by bi-linear interpolation from the action densities n_j at the surrounding discrete spectral points

$$n_i = \sum_{j=1}^{4} w_j n_j. \tag{54}$$

This procedure is visualised in Fig. 9. As shown in this figure, bi-linear interpolation is used to obtain the values for the action densities for the wave numbers $\vec{k}_2$ and $\vec{k}_4$. Note that no interpolation is necessary to obtain the action densities at the wave numbers $\vec{k}_1$ and $\vec{k}_3$. The action densities at the four wave numbers can then be used to compute the action density product term $N_{1,2,3,4}$.

4.3. Boundary conditions

In practise, the spectral grid is given for a set of wave numbers from $k_{\min}$ to $k_{\max}$. For points on the locus with a wave number smaller than $k_{\min}$ it is assumed that the action density is zero. For points on the locus with a wave number higher than $k_{\max}$ a parametric decay of the action density spectrum is assumed

$$n(k,\theta) = n(k_{\max},\theta)\left(\frac{k}{k_{\max}}\right)^p \quad \text{for} \quad k > k_{\max}. \tag{55}$$

The interpolation of the action density then simplifies to

$$n_i = \sum_{j=1}^{2} w_j n_j \left(\frac{k_i}{k_{\max}}\right)^p \tag{56}$$

in which the weights w_i reflect interpolation in direction. In the computational method, the term between the brackets is assimilated in the tail parameter t_i

$$t_i = \begin{cases} \left(\dfrac{k_i}{k_{\max}}\right)^p & \text{for} \quad k_i > k_{\max} \\ 1 & \text{for} \quad k_i \le k_{\max} \end{cases}. \tag{57}$$

In addition, when $k_i > k_{\max}$, the action density n_i is equal to the action density of the corresponding bin with $k = k_{\max}$.

4.4. Pre-processing

The pre-processing of the WRT method comprises the computation of the following information for each point on the locus:

- the indices of the lower left corner of the bin in the spectral grid, i_k and i_θ;
- the interpolation weights w_i, for $i = 1,4$;
- the tail factors t_i, for $i = 1,2$;
- the local step size Δs_i;
- the Jacobian term J_i;
- the coupling coefficient G_i.

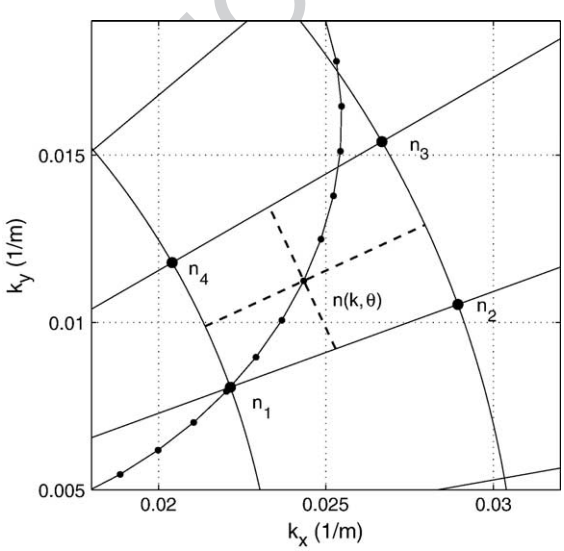

Fig. 9. Definition sketch for the bi-linear interpolation of action densities for points on the locus.

A useful property is that the loci, Jacobians and couplings coefficients are invariant to rotations of the generating wave number pair $\left(\vec{k}_1, \vec{k}_3\right)$. This property allows to reduce the amount of computations to determine the position and associated coefficients of each point on the locus. Transformation rules of loci are described in Tracy and Resio (1982).

An example of the functions that need to be integrated along a closed locus is shown in Fig. 10. For this example a standard JONSWAP spectrum with a $\cos^{2s}(\theta/2)$ directional distribution was used. It can be seen that the Jacobian term J, the coupling coefficient G and the wave number product $N_{1,2,3,4}$ are smooth functions. Therefore, the resulting compound function is also a smooth function.

An example of the integration of the functions along the locus for the special case (consisting of two straight lines) is shown in Fig. 11. This figure clearly shows that the Jacobian term increases quadratically with wave number. As noted in Section 2, the Jacobian term J becomes unbounded when $|\vec{c}_{g,2} - \vec{c}_{g,4}| \to 0$. For large wave numbers the increase in Jacobian term is counteracted by the decrease of the coupling coefficient and the action density product. The behaviour of the latter term is due to the fact that the action density decreases with increasing wave number according to a power law. The final function is limited, such that the contribution of the integral T remains bounded. Thus, the singularity in the Jacobian term occurs well outside the energy containing part of the spectrum.

It is noted that the contribution of the T terms for the special case only affects the directional distribution of the non-linear transfer rate, since energy is only exchanged between wave numbers with equal magnitude.

4.5. Extent of the discrete wave number grid

Applying the WRT-method, and likely any other exact computational method, to a discrete wave spectrum requires a sufficiently large frequency (or wave number) domain to ensure that the typical three-lobe structure of the non-linear transfer rate is retained. As shown by Young and Van Vledder (1993), the directionally integrated non-linear transfer rate for a mean JONSWAP spectrum, typically consists of two positive lobes, separated by a negative lobe that starts just above the peak frequency of the wave spectrum. With increasing frequency, the second positive lobe slowly decays to zero.

Various physical and numerical arguments apply to choose a sufficiently large frequency domain, bounded by a minimum and a maximum frequency, to ensure that the non-linear transfer rate is properly reproduced. Experience with the WRT method shows that for deep water the minimum frequency should at most be equal to half the peak frequency. The maximum frequency should be taken large enough such that the computed non-linear transfer rate satisfies the conservation laws for action, energy, and momentum. The precise maximum value with respect to the peak frequency of the spectrum

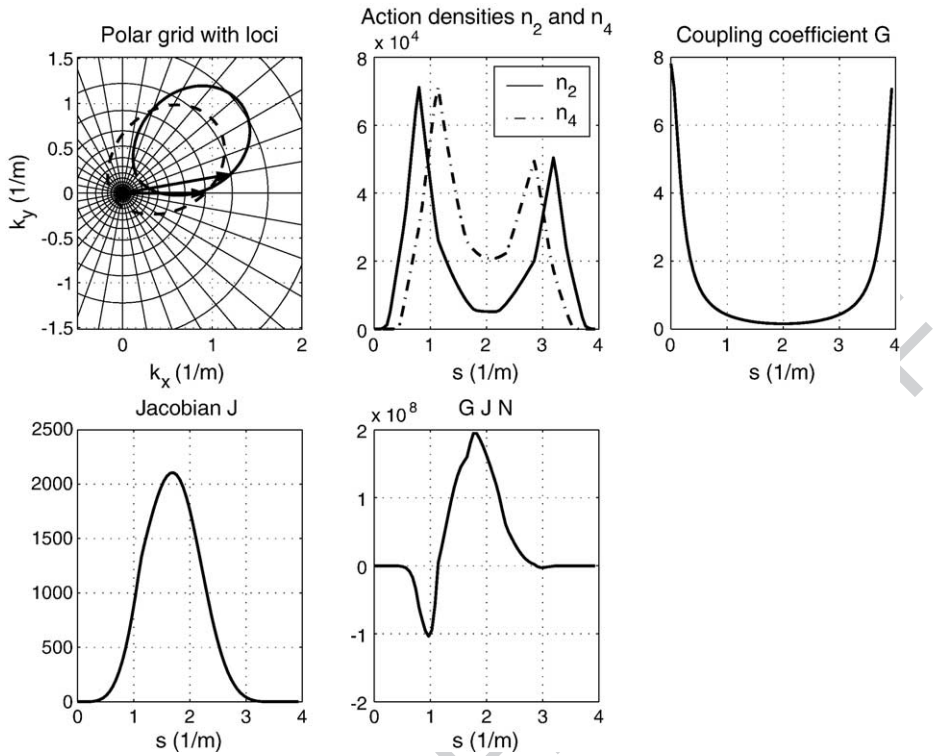

Fig. 10. Location of the locus in wave number space and the variation of the interpolated action densities, coupling coefficient and Jacobian term as a function of the local coordinate s.

depends on the peakedness of the spectrum, the required accuracy to satisfy these laws, and the power of the parametric tail in the host model. This implies that some trial and error is needed to determine this limit in wave evolution studies. Another physical argument is related to the ability of the non-linear four-wave interactions to generate a bi-modal distribu-

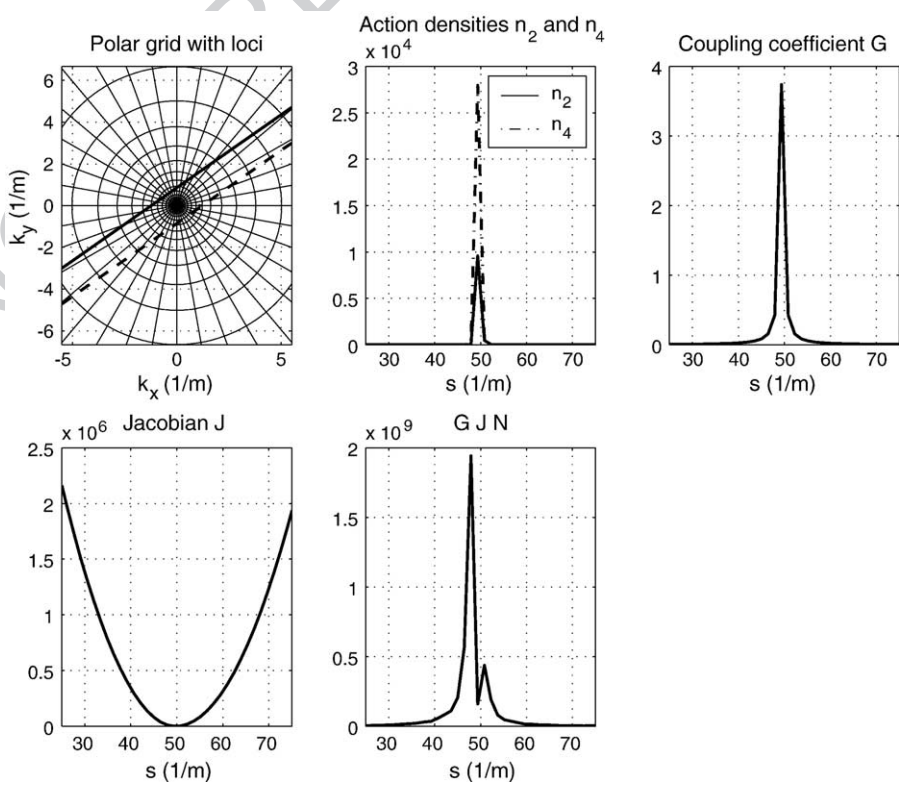

Fig. 11. Location of the loci in wave number space for the special case, and the variation of the interpolated action densities, coupling coefficient and Jacobian term as a function of the local coordinate s.

tion in wave growth situations for frequencies higher than two times the peak frequency (see Banner and Young, 1994). An example of this behaviour is given by Van der Westhuysen et al. (2004) who show that the WRT method is able to reproduce this bi-modal structure as observed by Hwang et al. (2000). Again, the choice of the upper limit depends on the requirements of the user.

A numerical argument of choosing a sufficiently high maximum frequency is related to cut-off effects near the upper boundary of the frequency (or wave number) grid. As follows from Eq. (50), the non-linear transfer rate in a certain spectral bin depends on all interactions with higher and lower frequencies. For the frequency bins near the maximum discrete frequency, only a limited amount of interactions with higher frequency bins is possible. Interactions with hypothetical bins, i.e. those with frequencies higher than $f_{\max}$ are not taken into account. This implies that the non-linear transfer rate of bins with frequencies near the maximum discrete frequency is inaccurate.

The magnitude of this cut-off effect is illustrated by the results of a series of computations with the WRT method for a discrete spectrum with increasing maximum frequency. In line with the current wave modelling practice, the directional resolution was 10°, and the frequency resolution was 10%, i.e. $f_{i+1}=1.1f_i$. In each subsequent computation a new frequency was added, while keeping the previous frequencies. In these computations the non-linear transfer rate was computed for a JONSWAP spectrum with a peak frequency of 1 Hz, a peak enhancement factor of 3.3, and an f^{-5} spectral tail. The directional distribution was a $\cos^{2s}(\theta/2)$ distribution with $s=2$. The computed directionally integrated non-linear transfer rates are shown in Fig. 12 as a function of the normalized frequency f/f_p. The dots in this figure are the end points of the non-linear transfer rate as computed up to a certain normalized frequency. The solid line represents the non-linear transfer rate as computed for a sufficiently high maximum frequency ($f_{\max}=10f_p$). The results clearly indicate that the cut-off effect vanishes when $f_{\max}>6f_p$. Computations with other spectral shapes (not shown here) support this conclusion. The results in Fig. 12 also imply that the non-linear transfer rate is affected by cut-off effects for the upper 20% of the discrete frequency range.

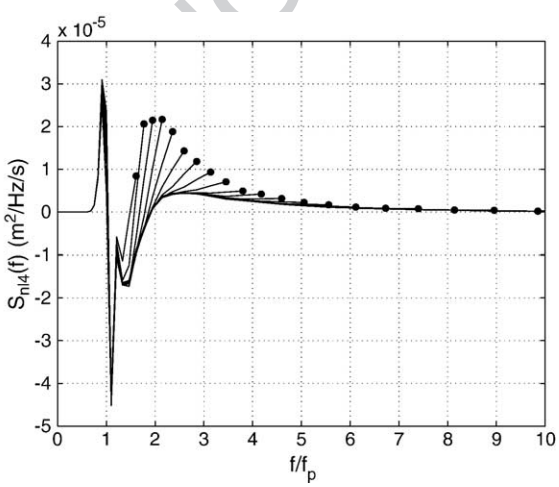

Fig. 12. Non-linear transfer rate for a JONSWAP spectrum with $\gamma=3.3$ computed with a varying maximum discrete frequency as a function of the normalized frequency f/f_p. The dots represent the computed non-linear transfer rate at the maximum discrete frequency.

5. Increasing the computational efficiency

5.1. Introduction

In the previous sections the theoretical and computational framework for the WRT method has been outlined. For many operational applications, savings in computational requirements are necessary, while retaining more or less the same accuracy. Here, a number of methods are described to reach this goal. For some methods computations have been performed to quantify their parameter settings and to quantify the gain in speed. In addition, some methods are proposed that may lead to a further speed-up of the WRT method.

5.2. Optimal number of points on the locus

To reach optimal accuracy the number of points on the locus must be large enough to ensure that all cells in a discrete spectrum have a few points along a locus. If a cell does not contain a discrete grid point, the integration procedure might miss relevant spectral information. On the other hand, too many locus points in a cell result in an inefficient integration procedure. Therefore, the distribution of discrete grid points along a locus must reflect the local resolution of the spectral grid, such that each cell contains at least one or two discrete points of the k_2-locus. Since the k_2- and k_4-loci are coupled, an optimal distribution of grid points on the k_2-locus is not necessarily optimal for the k_4-locus. Therefore, grid points need to be added along both loci to satisfy the requirement of at least one grid point in each cell.

As a first step to obtain an optimal distribution of points along the locus, computations were carried out with an equidistant spacing to determine the optimal number of points (using the fourth method described in Section 3.3 as illustrated in panel (d) of Fig. 6). In these computations the non-linear transfer rate was computed for 5 different JONSWAP spectra, with $\alpha=0.01$, $f_p=0.1$ Hz, an f^{-5} spectral tail, and with different peakedness factors, $\gamma=1$, 2, 3, 5 and 9, and a frequency dependent directional $\cos^{2s-}$ distribution according to Hasselmann et al. (1980). For each spectrum the non-linear transfer rate was computed with a different number of points on the locus N_{loc}, varying from 10, 15,. . ., 95, 100. For each spectrum and for each computation with a specific number of points, the relative error was computed using the directionally integrated non-linear transfer rates according to

$$\varepsilon=\frac{\sum_{i=1}^{N_f}|S_{nl}^{B}(f_i)-S_{nl}(f_i)|\Delta f_i}{\sum_{i=1}^{N_f}|S_{nl}^{B}(f_i)|\Delta f_i} \tag{58}$$

in which N_f is the number of frequencies, Δf_i the bandwidth per frequency, and where S_{nl}^{B} refers to the benchmark transfer rate,

i.e. the one based on 100 points on the locus. Next, the average relative error over all spectra was computed. The computed non-linear transfer rate of the JONSWAP spectrum with $\gamma=2$ for various values of N_{loc} is shown in panel (a) of Fig. 13. Panel (b) in this figure shows the average error (based on the results for all 5 test spectra) as a function of the number of points on the locus. The results indicate that the results have a relative error of at most 0.05 when the number of points exceeds 50.

5.3. Filtering

Filtering out insignificant contributions to the transfer integral can make significant savings in computational requirements. This technique was applied in the EXACT-NL model (Hasselmann and Hasselmann, 1985a) using a reference spectrum to detect these small contributions and to store the relevant contributions in a database. It is noted that the filtering in the EXACT-NL model depends on both the magnitude of the coupling coefficients and the actual spectral densities.

Resio (1998) introduced a filtering technique based on the distance in wave number space between the wave numbers $\vec{k}_1$ and $\vec{k}_3$. The reasoning behind this kind of filtering is that with increasing separation in wave number space, the coupling coefficient decreases, such that the contribution to the total transfer rate also decreases. Two criteria are used to omit a contribution of a T-term. The first criterion omits contributions when the highest ratio of k_1/k_3 or k_3/k_1 of the wave numbers k_1 and k_3 exceeds a threshold ratio k_R. The second one omits contributions when the angular difference $\Delta\theta_{1,3}=|\theta_1-\theta_3|$ exceeds a threshold difference θ_{max}. Similar to the previous analysis, computations were carried out to determine the optimum settings for the ratio k_R and angular difference θ_{max}. The results of this analysis are presented in the Figs. 14 and 15, respectively. The results indicate that similar non-linear transfer rates can be obtained by choosing $k_R=4$ and $\theta_{max}=60°$. This approach resembles the RIA method of Lin and Perrie (1998) who used mathematical arguments to restrict the integration space.

The gain in speed depends on the spectral resolution. Since the present computations were carried with a frequency spacing of 10% (for deep water equivalent to a wave number spacing of 21%) and a directional resolution of 10°, the gain in speed is a factor 3, for both types of filtering. Applying both types of filtering leads to a speedup of one order of magnitude.

In contrast to the EXACT-NL model, this type of filtering is independent of the spectral values. This implies that further savings can be obtained by introducing some type of filtering on the basis of the action densities at the wave numbers $\vec{k}_1$ and $\vec{k}_3$.

5.4. Geometric scaling

For various reasons it is convenient to use a geometric spacing of wave numbers in discrete spectral models, in which $k_{i+1}=\lambda k_i$ with $\lambda>1$. Such spacing provides a higher spectral resolution near the peak of the spectrum, and less resolution in the high-frequency tail. For deep water it also allows using scaling laws to derive the loci for related wave number pairs $\left(\vec{k}_1,\vec{k}_3'\right)$ and $\left(\lambda\vec{k}_1,\lambda\vec{k}_3\right)$. As shown by Tracy and Resio (1982) the size of the loci scales with λ, the coupling coefficient G scales with λ^6 and the Jacobian term J scales with λ. However, the action density product term $N_{1,2,3,4}$ does not scale.

Resio and Perrie (1991) indicated that this scaling technique speeds up the computation of the non-linear transfer rate by an order of magnitude compared to integration on regular spaced grids. However, this is only true when the loci are computed with each computation of the non-linear transfer rate and when deep water is considered. The gain in speed is limited because the product term of action densities cannot be scaled and needs to be evaluated for each locus. Common operational discrete spectral wave models like WAM, WaveWatch, TOMAWAC and SWAN, use a geometric spacing of the frequencies. For deep water, this results also in a geometric spacing of wave numbers. For finite depth however, this results in a non-geometric spacing

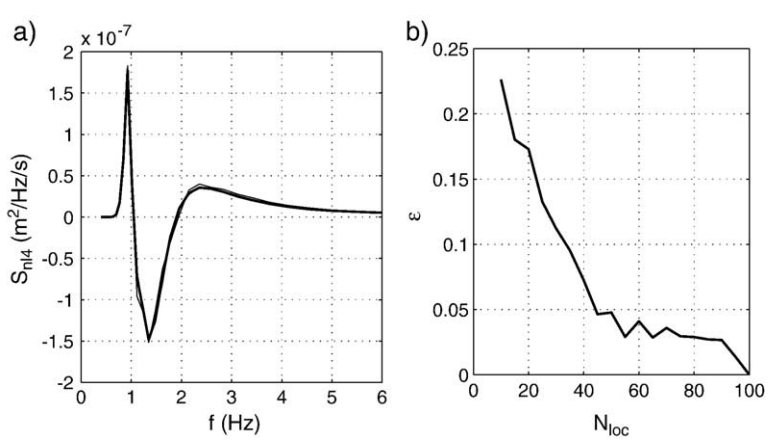

Fig. 13. Non-linear transfer rates for a JONSWAP spectrum with $\gamma=2$, computed with different values of N_{loc} (panel a). Thick line ($N_{loc}=100$), thin lines ($N_{loc}=20$ and 45). Average relative error of computed non-linear transfer rate as a function of the number of points on the locus N_{loc} (panel b). Average based on results of the 5 test spectra.

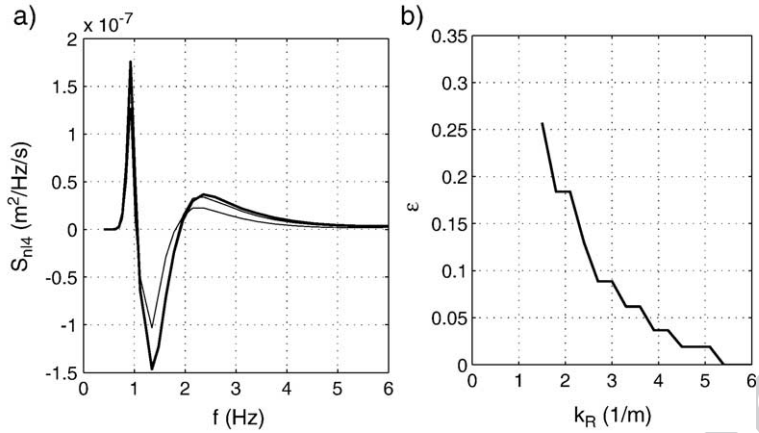

Fig. 14. Non-linear transfer rates for a JONSWAP spectrum with $\gamma=2$, computed with different values of k_R (panel a). Thick line ($k_R=6$), thin lines ($k_R=2$ and 4). Relative error of computed non-linear transfer rate as a function of the threshold value k_R (panel b).

for the wave numbers, and scaling relations cannot be used for the computation of the loci, associated Jacobians and coupling coefficients.

The only advantage of using geometric scaling for deep water is that it results in a smaller database of pre-computed values for a discretized integration space and interpolation coefficients, Jacobians and coupling coefficients. However, during the actual computation of the non-linear transfer rate, all interacting loci have to be considered and the loci and associated coefficients need to be obtained by re-scaling and rotating previously computed ones. Thus, the gain in computational speed is marginal.

When the integration space can be pre-computed, accuracy becomes more important than efficiency. Moreover, the positions of the discrete points on the locus become more important in view of their relation with the discrete spectral grid. This aspect is often neglected in the development of computational methods for determining the integration space.

5.5. Symmetry condition and compacting

As indicated in Section 2, the integration space can be reduced by a factor 2 by using the symmetry condition. This is expressed by the function, see the Eqs. (22) and (23). The reduction in integration space is compensated by a factor 2 in Eq. (24). When this option is in effect, part of the function along the locus does not contribute to the integral around the locus because the compound function now comprises the function $H(s)$, which has zero-values. To avoid adding zero contributions in the evaluation of the function, thereby omitting the potential gain in speed, the discrete points on the locus where $H(s_i)=0$ are identified in the pre-processing phase, and not stored in memory. This is achieved by compacting the pre-computed loci and associated coefficients. In this way, the actual integration only uses contributions on each locus where the function H is one, and a gain in speed with a factor 2 is obtained.

5.6. Bi-linear interpolation versus nearest bin approach

Experience shows that most of the workload is spent in the repeated bi-linear interpolation of action densities. This interpolation is based on the assumption that the action density varies linearly between the discrete corner points of a cell in wave number space. Following Snyder et al. (1993) the spectrum can also be represented as piece-wise constant, with

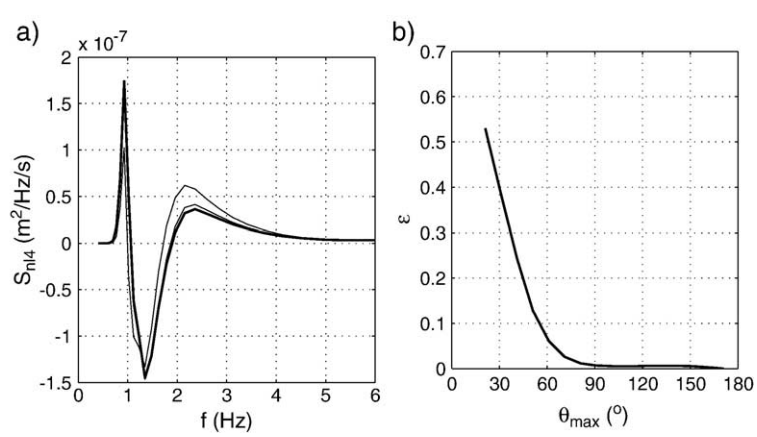

Fig. 15. Non-linear transfer rates for a JONSWAP spectrum with $\gamma=2$, computed with different values of θ_{max} (panel a). Thick line ($\theta_{max}=180°$), thin lines ($\theta_{max}=31°$ and 61°). Relative error of computed non-linear transfer rate as a function of the threshold value θ_{max} (panel b).

the discrete spectral grid point in the centre of the constant piece. This representation replaces the bi-linear interpolation with the nearest spectral grid point approach. This approach speeds up the computation by a factor of about 2, since the cumbersome bi-linear interpolation is replaced by direct retrieval of the action density at the nearest interacting wave number. Moreover, it reduces the size of the pre-computed integration space by 50% since the interpolation weights can be omitted. Fig. 16 shows a comparison of the WRT method using bi-linear interpolation and nearest-bin interpolation for a mean JONSWAP spectrum with a peak enhancement factor of $\gamma=2$. The computed error according to (58) is 0.14.

5.7. Higher order integration

The integration of the functions around the locus is basically the numerical integration of a tabulated function, viz. $G(s_i)J(s_i)N(s_i)$. In the present approach, a first order trapezoid rule is used to evaluate the integrals along the locus. It is likely that these integrals can be calculated more efficiently by using higher-order integration methods, such as the Simpson rule, or an n-point Gauss–Legendre quadrature method. Application of such methods requires full control of the spacing of the points on the locus, and a smooth behaviour of the compound function along the locus. The first requirement can easily be met by firstly computing a sufficiently fine (and optionally equidistant) distribution of points on the locus, followed by linear interpolation to the required spacing for these quadrature methods. In addition, the corresponding coupling coefficients and Jacobian terms need also be obtained by interpolation. As shown by Gorman (2003), the coupling coefficient needs to be computed only for exactly resonating wave numbers. Re-computation of the coupling coefficient based on interpolated wave numbers leads to small deviations of exact resonance, which in turn may lead to relatively large errors in the coupling coefficient. Therefore, no re-computation of the coupling coefficients should be performed. The second requirement is usually met since the action density in neighbouring spectral bins is coupled.

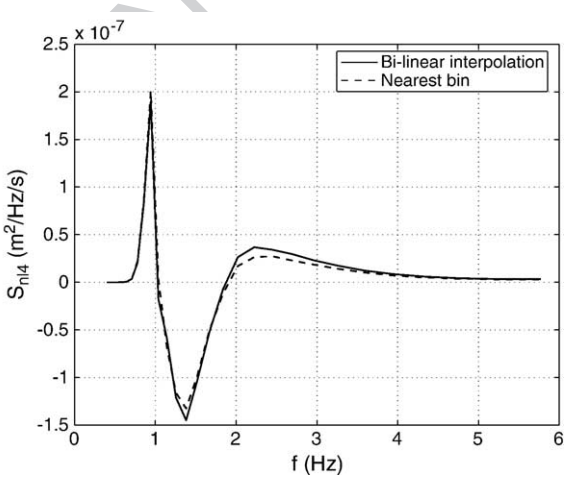

Fig. 16. Non-linear transfer rates for a JONSWAP spectrum with $\gamma=2$, computed with the WRT method using bi-linear interpolation (solid line) and nearest bin interpolation (dashed line). The relative error is 0.173.

6. Operational handling of the WRT method

6.1. Introduction

In the previous sections the WRT method for computing the non-linear transfer rate for a given discrete wave spectrum has been described in detail. The computational procedure for computing these interactions has been programmed in a set of routines, which are available as a set of subroutines. This allows easy implementation in any discrete spectral wave model. In this procedure the input consists of the characteristics of the spectral grid, the energy densities and the water depth. The output consists of the non-linear transfer rate on the same spectral grid. As long as this procedure is followed for a limited set of spectra, no special computational requirements are necessary. When applied in an operational discrete spectral wave model, various measures are needed to achieve acceptable computational requirements.

In this section the concepts of memory and disks are used to make a distinction between two types of memory, viz. the internal memory and the memory on disk, respectively. The first one is only used during the actual program application, and vanishes after program execution ends. The second type of memory refers to the permanent memory, such as hard disks. The precise wording of these types of memory may change as computer technology progresses.

Below various methods are described for an efficient application of the WRT method for computing the non-linear transfer rate in an operational wave prediction model. Attention is given to an optimal handling of pre-computed integration spaces.

6.2. Handling of pre-computed integration spaces in shallow water

An important property of the WRT method is that for a given discrete spectral grid and water depth, all loci, interpolation coefficients, coupling coefficients and Jacobian terms can be pre-computed and stored in memory or in a database on disk. During the actual computation of the non-linear source term for a discrete spectrum on this spectral grid, these pre-computed coefficients must be retrieved from memory and used in the actual computation.

In constant-depth applications the procedure is simple since only one integration space needs to be computed. In practise these data can be kept in memory. In variable-depth applications the procedure is more complicated since the non-linear transfer rate is depth dependent. Herterich and Hasselmann (1980) made an analysis of this effect; they showed that the magnitude of the transfer rate increases with decreasing water depth. Inspection of computational results obtained by Hasselmann and Hasselmann (1985a,b) with the EXACT-NL model shows that also the shape of the non-linear transfer rate changes. This effect is illustrated in Fig. 17 based on computations for a JONSWAP spectrum with $f_p=0.1$ Hz, $\alpha=0.0175$, an f^{-5} spectral tail, a peak enhancement factor of $\gamma=3.3$, and a $\cos^2(\theta)$ directional spreading. The main features

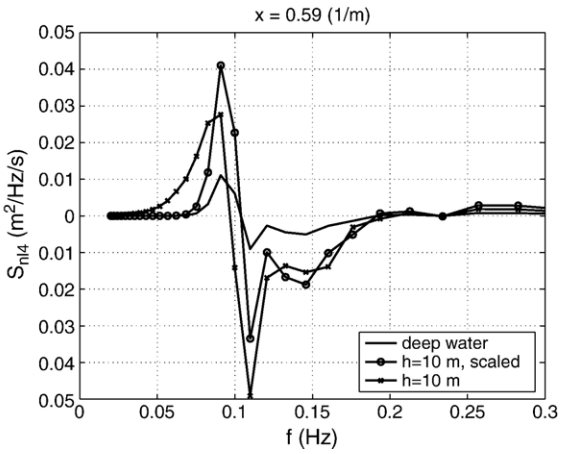

Fig. 17. Non-linear transfer rates for a JONSWAP spectrum with f_p=0.1 Hz, α=0.0175, γ=3.3 and a $\cos^2(\theta)$-directional spreading. WRT results for deep water (solid line), shallow water with h=10 m (line with crosses), and for shallow water with h=10 m using the WAM depth scaling (line with circles).

are an increase of the magnitude of the positive and negative peak values, an increase of the lower positive lobe, and a shift of the first zero-crossing to lower frequencies. Another feature is that the non-linear transfer rate is non-zero for frequencies exceeding 25% of the peak frequency. This implies that the minimum discrete frequency should be chosen accordingly.

In a typical finite-depth two-dimensional wave model application, the source terms are computed for each grid point in a certain countable progression. This implies that the integration space is possibly different for each subsequent grid point, and that it needs to be computed repeatedly. Storing all integration spaces in the internal memory is not always possible, due to memory restrictions.

This procedure can be simplified in a number of ways. The first simplification concerns the depth resolution. For instance, savings can be made to compute integration spaces only for rounded depth values, say, with a resolution of 1 m. A second option, not necessarily excluding the first option, is to store all required pre-computed integration spaces on disk. This may require the following procedure during an actual computation. For each grid point, a check is made whether a pre-computed integration space exists in memory for the depth in this grid point. If not in memory, a check is made if a proper integration space exists on disk. If this is the case, it is read in memory. If not, it is computed, saved to disk and stored in memory. The third simplification concerns sorting the spatial grid points with respect to their depth. Then, the integration space needs only to be re-computed and written to the two types of memory when a spatial grid point with a new (rounded) water depth is encountered in the sequence of spatial grid points.

Further savings can be made to compute the integration space only for a selected set of water depths. For instance in a geometric progression of, say, 1, 2, 4, . . . up to 1024 m, which can safely be considered as deep water. The spacing of these depths should be small enough to capture the essential changes in magnitude and shape of the non-linear transfer rate with depth. Then, during the actual wave model application for a given spatial grid point with a certain (target) water depth, the 'nearest' integration space is searched. A criterion to determine the nearest integration space, is to consider the relative differences of the target depth h with the depths for which an integration space have been pre-computed. Given a sequence of increasing depths, h_1, h_2, . . .h_N, a search is made for the pair of depths such that $h_i<h<h_{i+1}$. Then, the depth with the ratio nearest to h/h_i or h_{i+1}/h is selected.

This procedure can be refined using the depth scaling behaviour of the non-linear transfer rate. As noted by Herterich and Hasselmann (1980), the magnitude of the non-linear transfer rate scales as a function of the dimensionless water depth $k_p h$, with k_p the peak wave number. The magnitude scaling observed by Herterich and Hasselmann (1980) was parameterized by WAMDIG (1988) resulting in simple function $R(x)$ given by

$$R(x) = 1 + \frac{5.5}{x}\left(1 - \frac{6}{7}x\right)\exp\left(-\frac{5}{4}x\right). \tag{59}$$

with $x=k_p h$. To increase wave model robustness in case of arbitrarily shaped spectra, Komen et al. (1994) replaced the peak wave number k_p by .75k_m, in which k_m is the mean wave number defined as

$$k_m = \left(\frac{\iint k^{-\frac{1}{2}} E(f,\theta)\mathrm{d}f\mathrm{d}\theta}{\iint E(f,\theta)\mathrm{d}f\mathrm{d}\theta}\right)^{-2}. \tag{60}$$

The parameterisation (59) is applied in current third-generation wave prediction models as follows: for a given water depth the non-linear transfer rate is computed for deep water, followed by scaling with the factor R, equal for all spectral bins

$$S^h_{nl,4}(f,\theta) = R(x) S^\infty_{nl,4}(f,\theta). \tag{61}$$

The effect of applying (61) to a deep-water non-linear transfer rate is also shown in Fig. 16. As noted above, it can clearly be seen that this depth scaling does not account for frequency dependent scaling behaviour. Despite this shortcoming it can still be used to correct the magnitude of the non-linear transfer rate of the 'nearest' depth h_N according to

$$S^h_{nl,4}(f,\theta) = S^{h_N}_{nl,4}(f,\theta)\frac{R(0.75k_m h)}{R(0.75k_m h_N)}. \tag{62}$$

The combination of searching for the integration space of the 'nearest' depth and the WAM scaling provides an optimal mix of shape preservation and magnitude scaling.

6.3. Symmetric spectra

In many academic studies involving the computation of the non-linear transfer rate it is assumed that the spectrum is symmetric around a mean direction θ_m. Consequently, the non-linear transfer rate is also symmetric around this mean direction. In practise, this implies that the directional loop in expression (50) covers only 180°. In this way a speedup of a factor 2 can be obtained.

6.4. Sector grid

Another method to reduce the computational workload in evaluating the non-linear transfer rate is to assume that the spectrum is only defined on a sector around a mean direction, often in combination with a symmetric spectrum. In Resio and Perrie (1991), and Banner and Young (1994), a 1D-transect model with a directional sector of ±120° was used to study fetch-limited wave growth. In the actual computation of the non-linear transfer rate on a sector grid it is assumed that the action density outside this sector is zero. This happens when a part of the locus falls outside this sector. This allows for a speedup of about a factor 2.

However, in operational applications, spectra are generally not symmetric or have only energy in a certain sector. Further, Lavrenov and Ocampo-Torres (1999) showed that even in fetch-limited wave growth with a constant wind, energy is transferred by the non-linear four-wave interactions to directions opposing the wind direction. It is therefore recommended to compute the non-linear transfer rate always on the full circle.

6.5. The diagonal term

Various third-generation models, like WAM, WaveWatch and TOMAWAC, use a semi-implicit integration scheme (WAMDIG, 1988). This scheme requires a diagonal term to estimate the source term at the new time step, defined as

$$\Lambda(f_i,\theta_j) = \frac{\partial S(f_i,\theta_j)}{\partial E(f_i,\theta_j)}. \tag{63}$$

For the WRT method this diagonal term can be computed as

$$\begin{aligned}\Lambda\left(\vec{k}_1\right) &= \frac{\partial}{\partial n_1}\left[\mathrm{d}\vec{k}_3 \int \mathrm{d}s G(s) J(s) N(s)\right] \\ &= \int \mathrm{d}\vec{k}_3 \int \mathrm{d}s G(s) J(s) \left[\frac{\partial}{\partial n_1} N(s)\right].\end{aligned} \tag{64}$$

Since $N = n_1 n_3 (n_4 - n_2) + n_2 n_4 (n_3 - n_1)$ the contributions to the diagonal term for wave number $\vec{k}_1$ can be written as

$$\Lambda\left(\vec{k}_1\right) = \int \mathrm{d}\vec{k}_3 \int G(s) J(s) [n_3(n_4 - n_2) - n_2 n_4] \mathrm{d}s \tag{65}$$

and

$$\Lambda\left(\vec{k}_3\right) = \int \mathrm{d}\vec{k}_3 \int G(s) J(s) [n_1(n_4 - n_2) + n_2 n_4] \mathrm{d}s \tag{66}$$

for the associated contribution of wave number $\vec{k}_3$. These expressions have been implemented in the subroutine version of the WRT method and are used in the WaveWatch III model.

6.6. Spectral grid resolution

The WRT method uses two spectral grids for the wave numbers $\vec{k}_1$ and $\vec{k}_3$. These grids are usually equal to one another, but they may also be different. The resolutions of these grids might be different from the spectral grid of the host model. In the case that the resolutions differ, the wave spectrum of the host model needs to be converted to the resolutions of the WRT method to obtain the wave action densities n_1 and n_3. Similarly, the computed non-linear transfer rate needs to be converted to the resolution of the host model. These two-way interpolations introduce unwanted errors and should therefore be avoided.

Experience with the WaveWatch III model (Tolman, 2002) indicates that the resolution of the WRT method should preferably be the same as the one of the host model. When the host model is formulated in terms of frequencies, they need to be converted to wave numbers, including depth dependencies. Also, the directional step should be the same, preferably on the full circle.

Choosing a lower resolution of the grid for the WRT method might lead to instabilities because not all degrees of freedom of the discrete wave spectrum can be accounted for. Choosing a finer resolution for the WRT method might lead to spurious effects because the interpolated wave spectra are piece-wise constant. The non-linear interactions immediately reshape the spectrum locally to obtain a smooth curved variation of the action density. It is noted that the EXACT-NL model uses a much finer grid for the computation of the non-linear transfer rate than the one for the representation of the wave spectrum. Typical examples of computational results of this model show indeed some raggedness (cf. Hasselmann and Hasselmann, 1981).

7. Conclusions

A detailed overview is presented of the method of Webb (1978) for the computation of the non-linear four-wave interactions in a gravity wave spectrum. The starting point is the Boltzmann integral presented by Hasselmann (1962, 1963a,b). The choice and order of transformations leads to an attractive set of equations without a singularity in the energy containing part of the wave spectrum.

Based on the pioneering work of Tracy and Resio (1982), and Resio and Perrie (1991), a computational method is described to compute the non-linear transfer rate for a discrete wave spectrum. Therefore, this computational method is generally known as the WRT method. The WRT method is conceptually simple since it comprises the repeated integration of smooth functions along pre-computed paths in wave number space. Another attractive feature of Webb's method is that the equations and structure of the computational method are the same for deep water and for shallow water. This simplifies the computational procedure and the implementation in an operational wave prediction model considerably.

A good understanding of the intricacies of the computational procedure for the evaluation of the non-linear four-wave interactions in a discrete wave spectrum is important for the development of optimal methods that are both accurate and operationally attractive. The method of Webb (1978) and its implementation by Tracy and Resio (1982) provided an excellent starting point for developing such an optimal method.

Various methods are presented for computing the loci making up the integration paths in wave number space. All

of these methods are able to generate points on the locus. It is argued that differences in computational efficiency of these methods are not the critical issue, but that they must be able to produce a regular or sufficiently fine distribution of points along each locus, such that all spectral bins contain one or more points.

To overcome the large computational requirements of the computational method, various methods are described that may reduce the computational workload, thereby increasing their applicability in discrete spectral wave models. These methods are scalable since they retain the mathematical structure of Webb's method. In this paper, the basic concept of each method is described, and parameter settings are suggested. However, further studies are recommended to determine the optimal settings of the various criteria used in these methods. Specific points of attention are the optimal distribution of points on the locus, the use of higher order quadrature methods, the spectral resolution in frequencies and directions, and filtering based on the actual spectral densities.

Due to the strong non-linear behaviour of the source term for the four-wave interactions, small deviations in source term representation are no guarantee that a particular optimisation method produces similar results in model integrations compared to results obtained with the full solution. It is therefore recommended to test the applicability of each optimisation method in model integration runs.

An important property of the WRT method is the division of the computational workload in a pre-processing part and the actual integration for a given discrete wave spectrum. For a given discrete spectral grid and water depth, the integration space and associated interpolation coefficients, Jacobian terms and coupling coefficients can be pre-computed and used in subsequent computations. This technique is not only used in the EXACT-NL model, but also in the DIA. For a deep-water application the integration space needs to be computed only once. For shallow water, many integration spaces need to be pre-computed. To increase the operational efficiency in a typical shallow water wave model application, a method has been proposed to efficiently handle the integration spaces for different water depths.

Despite the fact that application of these methods may lead to considerable savings in computational requirements, no claims are made regarding their efficiency in comparison with other computational methods. Such claims can only be made under controlled conditions. Moreover, the actual computational requirements strongly depend on details of the computational method and on the computer hardware.

The WRT method has been implemented in various operational wave prediction models, such as WaveWatch III, SWAN, CREST and PROWAM. This was achieved by developing a set of generally applicable routines that can be called as a subroutine from the host wave prediction model. The WRT method has been used in various studies regarding the source term balance in academic situations (Van Vledder and Bottema, 2002) and in field (Van der Westhuysen et al., 2004; Ardhuin et al., submitted for publication) yielding improved spectral shapes and growth behaviour.

Acknowledgements

The present paper is the result of a series of studies regarding the modelling of the non-linear quadruplet interactions in discrete wave spectra. This series started with ONR's Advanced Wave Prediction Program, contract N00014-98-C-0009, followed by the SWAN physics plus project, carried out jointly with WL|Delft Hydraulics for the Dutch Ministry of Transport and Public Works, contract RKZ-1018A. Funding was also obtained from the French Naval Oceanographic Centre (SHOM) in Brest. All their support is greatly acknowledged.

Special thanks are for Klaus and Susanne Hasselmann who introduced me to the secrets of the DIA and the EXACT-NL model. Don Resio and Barbary Tracy introduced me to their computational method of solving Webb's equations. Ian Young is acknowledged for our discussions on the nature and properties of the non-linear four-wave interactions.

The computational method presented in this paper was incorporated into various operational models. This was not possible without the help of Hendrik Tolman of NOAA/NCEP regarding the WaveWatch model, and IJsbrand Haagsma, Leo Holthuijsen, André van der Westhuysen and Marcel Zijlema of Delft University of Technology, regarding the implementation in the SWAN model. Fabrice Ardhuin of SHOM helped with the implementation in the CREST model, and Pedro Osuna and Judith Wolf of Proudman Oceanographic Laboratories did so regarding the PROWAM model.

Further, I thank the following colleagues who participated in discussions about the modelling of the non-linear four-wave interactions: Michael Banner, Michel Benoit, Richard Gorman, Noriaki Hashimoto, Tom Herbers, Bob Jensen, Igor Lavrenov, Vlad Polnikov, Andrei Pushkarev, Jørgen Rasmussen, Kaha Tsagareli, and Vladimir Zakharov.

Finally, I thank Jurjen Battjes for his continuing interest in these studies and his valuable comments on an early version of this paper.

Appendix A. Derivation of the Jacobian term in Cartesian coordinates

Tracy and Resio (1982) presented expression (21) in Cartesian coordinates

$$J = \left\{ \left(\frac{\partial \Delta\omega_{1,2,3,\vec{k}_1+\vec{k}_2-\vec{k}_3}}{\partial k_{2,x}} \right)^2 + \left(\frac{\partial \Delta\omega_{1,2,3,\vec{k}_1+\vec{k}_2-\vec{k}_3}}{\partial k_{2,y}} \right)^2 \right\}^{-1/2} . \tag{A1}$$

The partial derivatives in (A1) can be expressed as

$$\frac{\partial \Delta\omega_{1,2,3,\vec{k}_1+\vec{k}_2-\vec{k}_3}}{\partial k_{2,x}} = \frac{\sqrt{g}k_{2,x}}{2k_2^{3/2}} - \frac{\sqrt{g}k_{4,x}}{2k_4^{3/2}} \tag{A2}$$

with the wave number magnitude given by $k_i = |\vec{k}_i|$ and likewise for the y-component (it is noted that the factor $\sqrt{g}$ was

set to one in their equations). Van Vledder (2000) presented the finite depth versions of these equations, as they appear in the finite depth version of the WRT code of Resio (1998).

$$\frac{\partial \Delta\omega_{1,2,3,\vec{k}_1+\vec{k}_2-\vec{k}_3}}{\partial k_{2,x}} = \frac{g}{2\omega_2}\frac{k_{2,x}}{k_2}\left[\tanh(k_2h)+\frac{k_2h}{\cosh^2(k_2h)}\right] - \frac{g}{2\omega_4}\frac{k_{4,x}}{k_4}\left[\tanh(k_4h)+\frac{k_4h}{\cosh^2(k_4h)}\right] \quad \text{(A3)}$$

and likewise for the y-component. Expression (A3) can be simplified considerably by writing

$$\frac{k_{i,x}}{k_i} = \cos(\theta_i) \quad \text{(A4)}$$

and by writing the expression for the group velocity c_{gi} of the wave number k_i as

$$\frac{g}{2\omega_i}\left[\tanh(k_ih)+\frac{k_ih}{\cosh^2(k_ih)}\right] = c_{g,i}. \quad \text{(A5)}$$

Substituting the expressions (A4) and (A5) in expression (A1) and its y-equivalent, gives after some algebraic manipulations

$$J = \left(c_{g,2}^2 + c_{g,4}^2 - 2c_{g,2}c_{g,4}\cos(\theta_2-\theta_4)\right)^{-1/2} = |\vec{c}_{g,2} - \vec{c}_{g,4}|^{-1}. \quad \text{(A6)}$$

References

Ardhuin, F., Herbers, T.H.C., O'Reilly, W.C., 2001. A hybrid Eulerian–Lagrangian model for spectral wave evolution with application to bottom friction on the continental shelf. J. Phys. Oceanogr. 31 (6), 1498–1516.

Ardhuin, F., Herbers, T.H.C., Van Vledder, G.Ph., Watts, K.P., Jensen, R.E., Graber, H.C., submitted for publication. Swell and slanting fetch effects on wind wave growth. J. Phys. Oceanogr.

Banner, M.L., Young, I.R., 1994. Modeling spectral dissipation in the evolution of wind waves: Part 1. Assessment of existing model performance. J. Phys. Oceanogr. 24, 1550–1570.

Benoit, M., 2005. Evaluation of methods to compute the nonlinear quadruplet interactions for deep-water wave spectra. Proc. 5th ASCE Int. Symp. on Ocean Waves, Measurements and Analysis, Madrid, Spain.

Benoit, M., Marcos, F., Becq, F., 1996. Development of a third generation shallow-water wave model with unstructured spatial meshing. Proc. 25th Int. Conf. on Coastal Eng., Orlando, Florida, pp. 465–478.

Booij, N., Ris, R.C., Holthuijsen, L.H., 1999. A third generation wave model for coastal regions: Part I. Model description and validation. J. Geophys. Res. 104 (C4), 7649–7666.

Booij, N., Haagsma, IJ.G., Holthuijsen, L.H., Kieftenburg, A.T.M.M., Ris, R.C., Van der Westhuysen, A.J., Zijlema, M., 2004. SWAN User Manual, SWAN Cycle III, Version 40.41. Delft University of Technology.

Dungey, J.C., Hui, W.H., 1979. Nonlinear energy transfer in a narrow gravity-wave spectrum. Proc. R. Soc. Lond. A368, 239–265.

Gorman, R., 2003. The treatment of discontinuities in computing the nonlinear energy transfer for finite-depth gravity wave spectra. J. Atmos. Ocean. Technol. 20 (1), 206–216.

Hashimoto, N., Kawaguchi, K., 2001. Extension and modification of the Discrete Interaction Approximation (DIA) for computing nonlinear energy transfer of gravity wave spectra. Proc. 4th ASCE Int. Symp. on Ocean Waves, Measurement and Analysis, San Francisco, pp. 530–539.

Hashimoto, N., Tsuruya, H., Nakagawa, Y., 1998. Numerical computations of the nonlinear energy transfer of gravity-wave spectra in finite water depth. Coast. Eng. J. 40 (1), 23–40. (Japanese journal English language).

Hashimoto, N., Haagsma, IJ.G., Holthuijsen, L.H., 2002. Four-wave interactions in SWAN. Proc. 28th Int Conf. on Coastal Eng., Cardiff, pp. 392–404.

Hasselmann, K., 1962. On the non-linear energy transfer in a gravity-wave spectrum: Part 1. General theory. J. Fluid Mech. 12, 481–500.

Hasselmann, K., 1963a. On the non-linear energy transfer in a gravity-wave spectrum: Part 2. Conservation theorems; wave-particle analogy; irreversibility. J. Fluid Mech. 15, 273–281.

Hasselmann, K., 1963b. On the non-linear energy transfer in a gravity-wave spectrum: Part 3. Evaluation of energy flux and swell-sea interaction for a Neumann spectrum. J. Fluid Mech. 15, 385–398.

Hasselmann, K., Hasselmann, S., 1981. A symmetrical method of computing the non-linear transfer in a gravity wave spectrum. Hamburger Geophys. Einzelschriften, p. 52.

Hasselmann, S., Hasselmann, K., 1985a. The wave model EXACT-NL. Ocean Wave Modelling, The SWAMP group. Plenum Press, New York, 256 p.

Hasselmann, S., Hasselmann, K., 1985b. Computation and parameterizations of the nonlinear energy transfer in a gravity-wave spectrum: Part 1. A new method for efficient computations of the exact nonlinear transfer integral. J. Phys. Oceanogr. 15, 1369–1377.

Hasselmann, D.E., Dunckel, M., Ewing, J.A., 1973. Directional wave spectra observed during JONSWAP. J. Phys. Oceanogr. 10, 1264–1280.

Hasselmann, S., Hasselmann, K., Allender, J.A., Barnett, T.P., 1985. Computations and parameterizations of the non-linear energy transfer in a gravity-wave spectrum: Part 2. Parameterizations of the non-linear transfer for application in wave models. J. Phys. Oceanogr. 15, 1378–1391.

Herterich, K., Hasselmann, K., 1980. A similarity relation for the non-linear energy transfer in a finite-depth gravity-wave spectrum. J. Fluid Mech. 97, 215–224.

Hunt, J.N., 1979. Direct solution of the wave dispersion equation. J. Waterw., Port, Coast., Ocean Div., ASCE 105 (WW4), 457–459.

Hwang, P.A., Wang, D.W., Walsh, E.J., Krabill, W.B., Shift, R.N., 2000. Airborne measurements of the wavenumber spectra of ocean surface waves: Part 2. Directional distribution. J. Phys. Oceanogr. 30, 2768–2787.

Khatri, S.K., Young, I.R., 1999. A new technique to evaluate nonlinear wave interactions for ocean wave prediction models. Proc. 5th Int. Conf. on Coastal and Port Engineering in Developing Countries, Cape Town, South Africa, 19–23, pp. 159–169.

Komen, G.J., Cavaleri, L., Donelan, M., Hasselmann, K., Hasselmann, S., Janssen, P.A.E.M., 1994. Dynamics and Modelling of Ocean Waves. Cambridge University Press, 532 p.

Lavrenov, I.V., 2001. Effect of wind wave parameter fluctuation on the nonlinear spectrum evolution. J. Phys. Oceanogr. 31. , 861–873.

Lavrenov, I.V., Ocampo-Torres, F.J., 1999. Angular distribution effect on weakly nonlinear energy transfer in the spectrum of wind waves. Izv., Atmos. Ocean. Phys. 35 (2), 254–265 (English Translation).

Lin, R.Q., Perrie, W., 1998. On the mathematics and approximation of the nonlinear wave–wave interactions. In: Perrie, W. (Ed.), Nonlinear Ocean Waves, Advances in Fluid Mechanics, vol. 17. Comp. Mech. Publ, Southampton (UK), pp. 61–88.

Masuda, A., 1980. Nonlinear energy transfer between wind waves. J. Phys Oceanogr. 10. , 2082–2093.

Monbaliu, J., Hargreaves, J.C., Carretero, J.-C., Gerritsen, H., Flather, R., 1999. Wave modelling in the PROMISE project. Coast. Eng. 37, 379–407.

Phillips, O.M., 1981. Wave interactions–the evolution of an idea. J. Fluid Mech. 106. , 215–227.

Polnikov, V.G., 1997. Nonlinear energy transfer through the spectrum of gravity waves for the finite depth case. J. Phys. Oceanogr. 27. , 1481–1491.

Prabhakar, V., Pandurangan, J., 2004. A polar method for obtaining resonating quadruplets in computation of nonlinear wave–wave interactions. Proc. 3rd Indian National Conference on Harbour and Ocean Engineering, NIO, Goa, India, 7–9 December, pp. 443–448.

Rasmussen, J.H., 1998, Deterministic and Stochastic Modeling of Surface Gravity Waves in Finite Depth, Ph.D. Thesis, ISVA, Denmark, 245 pp.

Resio, D.T., 1998. Personal communication.

Resio, D.T., Perrie, W., 1991. A numerical study of nonlinear energy fluxes due to wave-wave interactions. Part 1: Methodology and basic results. J. Fluid Mech. 223, 609–629.

Resio, D.T., Pihl, J.H., Tracy, B.A., Vincent, C.L., 2001. Non-linear energy fluxes and the finite depth equilibrium range wave spectra. J. Geophys. Res. 106 (C4), 6985–7000.

Snyder, R.L., Thacker, W.C., Hasselmann, K., Hasselmann, S., Barzel, G., 1993. Implementation of an efficient scheme for calculating nonlinear transfer from wave–wave interactions. J. Geophys. Res. 98 (C8), 14507–14525.

Tolman, H.L., 1991. A third-generation model for wind waves on slowly varying, unsteady, and inhomogeneous depths and currents. J. Phys. Oceanogr. 21, 782–797.

Tolman, H.L., 2002. User Manual and System Documentation of WAVEWATCH III Version 2.22. Technical Report 222, NOAA/NWS/NCEP/MMAB, 133 pp.

Tolman, H.L., 2004. Inverse modeling of Discrete Interaction Approximations for nonlinear interactions in wind waves. Ocean Model. 6, 405–422.

Tracy, B.A., Resio, D.T., 1982. Theory and Calculation of the Nonlinear Energy Transfer Between Sea Waves in Deep Water. WIS Technical Report 11. US Army Engineer Waterways Experiment Station, Vicksburg, Mississippi, USA, 47 pp.

Van Vledder, G.Ph., 2000. Improved method for obtaining the integration space for the computation of non-linear quadruplet wave–wave interactions. Proc. 6th Int. Conf. on Wave Forecasting and Hindcasting, Monterey, California, USA.

Van Vledder, G.Ph., 2001. Extension of the Discrete Interaction Approximation for computing nonlinear quadruplet wave–wave interactions in operational wave models. Proc. 4th ASCE Int. Symp. on Ocean Waves, Measurements and Analysis, San Francisco, California, USA, pp. 540–549.

Van Vledder, G.Ph., Bottema, M., 2002. Improved modelling of nonlinear four-wave interactions in shallow water. Proc. 28th Int. Conf. on Coastal Eng., Cardiff, pp. 459–471.

Van Vledder, G.Ph., Weber, S.L., 1988. Guide to the program EXACT-NL. Max-Planck-Institut für Meteorologie, Hamburg, Germany. Report no. 20.

Van Vledder, G.Ph., Holthuijsen, L.H., 1993. The directional response of ocean waves to turning wind. J. Phys. Oceanogr. 23 (2), 177–192.

Van Vledder, G.Ph., Herbers, T.H.C., Jensen, R.E., Resio, D.T., Tracy, B.A., 2000. Modelling of non-linear quadruplet wave–wave interactions in operational wave models. Proc. 27th Int. Conf. on Coastal Engineering, Sydney, pp. 797–811.

Van der Westhuysen, A.J., Zijlema, M., Battjes, J.A., 2004. Improvement of the numerics and deep-water physics in an academic version of SWAN. Proc. 29th Int. Conf. on Coastal Eng., Lisbon, Portugal, pp. 855–867.

WAMDIG, 1988. The WAM model—a third generation ocean wave prediction model. J. Phys. Oceanogr. 18, 1775–1810.

Webb, D.J., 1978. Nonlinear transfer between sea waves. Deep-Sea Res. 25, 279–298.

Weber, S.L., 1988. The energy balance of finite depth gravity waves. J. Geophys. Res. C93, 3601–3607.

Young, I.R., Van Vledder, G.Ph., 1993. A review of the central role of non-linear interactions in wind-wave evolution. Philos. Trans. R. Soc. Lond. A342, 505–524.

Zakharov, V.E., 1968. Stability of periodic waves of finite amplitude on the surface of deep fluid. PMTF Zh. Prikl. Mekh. Tekh. Fiz. 3, 80–94.

Zakharov, V.E., 1999. Statistical theory of gravity and capillary waves on the surface of a finite-depth fluid. Eur. J. Mech. B, Fluids 18 (3), 327–344.

Gerbrant van Vledder studied Civil Engineering at Delft University of Technology. In 1983 he received his master degree on the topic of a statistical analysis of random wave groups. In 1990 he received his Ph.D. on the topic of the directional response of wind waves to turning winds. From 1988 till 1996 he was employed at WL|Delft Hydraulics as a hydraulic engineer. Since 1996 he is an employee of Alkyon Hydraulic Consultancy and Research. His main activities are wave modelling, wave climate studies and the determination of Hydraulic Boundary conditions for dikes and offshore structures.